



140
986
THS

1
2008

**LIBRARY
Michigan State
University**

This is to certify that the
dissertation entitled

**POLYELECTROLYTE MULTILAYER COATINGS FOR
CONDUCTIVE NANOMATERIALS PATTERNING AND ANTI-
WRINKLING APPLICATIONS**

presented by

Troy Richard Hendricks

has been accepted towards fulfillment
of the requirements for the

Doctoral degree in Chemical Engineering



Major Professor's Signature

4/15/08

Date

PLACE IN RETURN BOX to remove this checkout from your record.
TO AVOID FINES return on or before date due.
MAY BE RECALLED with earlier due date if requested.

DATE DUE	DATE DUE	DATE DUE

**POLYELECTROLYTE MULTILAYER COATINGS FOR CONDUCTIVE
NANOMATERIALS PATTERNING AND ANTI-WRINKLING APPLICATIONS**

By

Troy Richard Hendricks

A DISSERTATION

**Submitted to
Michigan State University
in partial fulfillment of the requirements
for the degree of**

DOCTOR OF PHILOSOPHY

Department of Chemical Engineering

2008

co

su

al

or

th

a

a

H

ty

s

c

th

e

s

F

e

Abstract

POLYELECTROLYTE MULTILAYER COATINGS FOR CONDUCTIVE NANOMATERIALS PATTERNING AND ANTI-WRINKLING APPLICATIONS

By

Troy Richard Hendricks

Layer-by-layer assembly oppositely charge polymers to form thin films containing polyelectrolyte multilayers (PEM) can be used to significantly alter surface properties and control the chemical functionality of a surface. The alternate adsorption of oppositely charged poly-ion molecules can be performed on virtually any surface and creates an ultra thin film that has different properties than the substrate on which the films are formed. In this research, PEM are used as platforms for patterning conductive materials for future electronic devices and as model films to investigate nano-mechanical properties of the PEM films.

Flexible electronic devices are the goal in current microelectronics research. However, the current fabrication methods, mainly photolithography, limit the types of materials which can be used and do not allow for flexible or non-planar substrates to be patterned. In this research, PEM are used as platforms and are combined with microcontact printing (μ CP) to pattern conductive materials. First, the combination of PEM and μ CP are used to create copper patterns using electroless deposition. The resulting copper patterns are found to be highly selective and can be used to pattern multiple types of substrates. Secondly, PEM and μ CP are used with poly(amidoamine) dendrimers to investigate the effect of the catalyst introduction method on the electroless deposition of nickel.

Th

m

als

us

are

pa

co

Wh

F

po

rub

or

the

sys

the

The catalyst introduction method was shown to affect the selectivity and morphology of the resulting nickel patterns. The number of PEM bilayers was also shown to affect the selectivity of nickel deposition. Lastly, PEM and μ CP are used to pattern exfoliated graphite nanoplatelets (xGnP). The conductive xGnP are used to replace the less flexible metal used in the earlier studies. Conductive patterns of xGnP can be created by performing layer-by-layer assembly of PEM containing graphite onto the stamp before transferring to a PEM coated surface. When enough layers of xGnP are used the patterns become conductive.

PEM samples are used as a model to study the mechanical buckling of the polymer film onto a more elastomeric substrate. First, PEM are deposited onto a rubber substrate. Buckling or wrinkling occurs when the substrate is compressed or heated in an oven and then cooled. The addition of silica nanoparticles into the PEM film has been shown to prevent the composite films from buckling. This system is a basic model of human skin and creates a large amount of interest in the prevention of wrinkling.

**Copyright by
TROY RICHARD HENDRICKS
2008**

**To My Wife:
Anna Hendricks**

A

V

d

M

a

m

la

S

ec

S

at

M

mi

I

Fin

en

SECRET

Acknowledgments

First, I would like to thank Prof. Ilsoon Lee for his support and guidance. Without his patience I would not have been able to successfully complete my degree. I would also like to thank Prof. Patrick Kwon, Prof. Andre Lee and Prof. Mark Worden for serving on my committee and providing me with constructive advice and enthusiasm for my research. I would also like to thank the other members of my research group, especially Dr. Jue Lu for helping me with the layer-by-layer assembly of exfoliated graphite nanoplatelets.

I would also like to thank the members of the Composite Materials and Structures Center at MSU for their training, guidance and upkeep of the equipment. Specifically Dr. Per Askland for his help with the Environmental Scanning Electron Microscope and Dr. Hazel-Ann Hosein for her help with the atomic force microscope. I would also like to thank the Center for Advanced Microscopy for the help with obtaining scanning and transmission electron microscope images.

I would like to thank my parents for a lifetime of encouragement and support. Finally I would like to thank my wife Anna for her endless patience, encouragement, support and time spent proofreading.

Li
Li
Ch
Ch
Us

Ch
on

Cha
Nan

Cha
App

Ref

Table of Contents

List of Tables.....	viii
List of Figures.....	ix
Chapter 1: Introduction to Polyelectrolyte Multilayers	1
Chapter 2: A Versatile Approach to Selective and Inexpensive Copper Patterns Using Polyelectrolyte Multilayer Coatings	6
Introduction	6
Experimental Details	9
Results and Discussion.....	13
Conclusion	20
Chapter 3: Effects of Catalyst Introduction Methods Using PAMAM Dendrimers on Selective Electroless Nickel Deposition on Polyelectrolyte Multilayers	21
Introduction	21
Experimental Details	23
Results and Discussion.....	26
Conclusion	39
Chapter 4: Direct Transfer of Patterned Polymer/Graphite Conductive Nanocomposite Films to Polyelectrolyte Multilayer Platforms	40
Introduction	40
Experimental Details	42
Results and Discussion.....	44
Conclusion	50
Chapter 5: Control and Prevention of Polymer Film Buckling for Anti-wrinkling Applications.....	51
Introduction	51
Experimental Details	54
Results and Discussion.....	56
Conclusion	74
References.....	75

List of Tables

Table 1: Summary of the three different catalyst introduction methods	24
Table 2: Summary of buckling data for plasma treated PDMS substrates with no PEM films	59
Table 3: Summary of buckling data for PEM films on PDMS substrates	64

Fi
co

Fi
pa

Fi
co
po
pa
the
su

Fig
pat
sub

Fig
sho
calc

Fig
cata

Fig
dep
enc
resp

Fig
patt
patt
micr
PAN
(c)..

Fig
gen
nan

List of Figures

- Figure 1:** Schematic illustration of LbL assembly and chemical structure for common strong (PDAC and SPS) and weak (PAH and PAA) polyelectrolytes.....2
- Figure 2:** Schematic of the overall fabrication process to create selective copper patterns on PEM coated substrates followed by colloidal deposition.....13
- Figure 3:** Reflected light optical micrographs of selective copper lines on PEM coated substrates. Parts (a) and (b) have glass substrates while (c) is on a polystyrene substrate. (d) Transmitted light optical micrograph of polystyrene particles deposited on the active unpatterned regions of the PEM surface next to the black copper lines. (e) A PEM coated flexible polyester transparency film substrate with electroless copper patterns which are ~30 nm thick.....15
- Figure 4:** AFM images of (a) a 20 μm x 20 μm image of selective copper patterns and (b) a 30 μm x 30 μm image of multilevel structure created by stamping a substrate twice before electroless deposition.....17
- Figure 5:** SEM image selectively plated copper lines on PEM. The EDS spectra shown are for the copper lines and the unpatterned polymer surface. The calcium peak was left to show the relative size of the copper peak.....18
- Figure 6:** QCM results of copper thickness versus time for homogeneously catalyzed and uncatalyzed surfaces.....19
- Figure 7:** Process schematic for the three different methods. Methods 1-3 are depicted in parts a-c, respectively. Diagrams of the dendrimer and dendrimer-encapsulated nanoparticle structures are also included in parts b and c, respectively.....27
- Figure 8:** Optical microscope and AFM images of G4 PAMAM dendrimer patterns on PEM. (a) Phase contrast optical microscope images of two different pattern types with (large) and without (inset) a blue filter, (b) fluorescence microscope image of FITC-labeled PAMAM, (c) topographical AFM image of PAMAM patterns, and (d) sample line scan taken from the AFM image shown in (c).....28
- Figure 9:** (a) TEM image of palladium nanoparticles fabricated in fourth generation PAMAM dendrimers. (b) Size distribution of the palladium nanoparticles.....30

Figure 10: Optical microscope images of electroless-deposited nickel patterns. (a) and (b) Bright-field images of direct catalyst stamping (method 1) and DA (method 2) respectively. (c) Dark-field images of dendrimer-encapsulated nanoparticles (method 3). The insets show a larger sample area and have a 20 μm scale bar. (d) Dark-field microscope image of electroless-deposited nickel patterns created by μCP ions encapsulated in dendrimers. The ions were not reduced to nanoparticles before stamping.....	31
Figure 11: AFM images of nickel patterns using methods 1 (a), 2 (b), and 3 (c).....	33
Figure 12: SEM images of patterned nickel samples created by methods 1 (a) and 2 (b). These images are accompanied with EDS spectra for the metal and polymer surfaces.....	35
Figure 13: Optical microscope images of samples created using DA (method 2). The number of bilayers affects the selectivity and quality of the deposited nickel patterns. The scale bar is valid for all images.....	36
Figure 14: QCM data for homogeneous surfaces that represent the different regions on the patterned surfaces.....	38
Figure 15: Illustration of the process to form xGnP, subsequent film formation on PDMS and transfer to a PEM coated substrate.....	44
Figure 16: (a) Optical microscope and (b) SEM images of PAH/(xGnP-SPS/PDAC) ₄ films transferred to a PEM coated substrate.....	46
Figure 17: Fluorescence microscope images of PDMS stamps coated with PAH/(xGnP-SPS/PDAC) ₄ films and dyed with 6CF (a) before and (b) after stamping. (c) An optical microscope image of a stamp after the film is transferred.....	48
Figure 18: Surface resistance vs. Frequency for various films on PDMS and films transferred to PEM surfaces.....	49
Figure 19: AFM images of flat PDMS substrates after (a) plasma treatment only, (b) plasma treatment and thermal processing the same day, (c) plasma treatment and overnight storage in air followed by thermal processing and (d) plasma treatment and storage in DI water overnight followed by thermal processing.....	56
Figure 20: Cross-sectional illustration of a silica film generated by oxygen plasma treatment (top) and a PEM film (bottom), before and after thermal processing.....	57

Figure 21: Optical microscope and AFM images of a buckled (PAH/PAA)_{5.5} film on a PDMS substrate after thermal processing. The smooth buckling morphology was caused by a mismatch in thermal expansion between the film and the substrate. (a) bright-field and (b) dark-field optical microscope images. (c) and (d) are 2D and 3D tapping mode AFM images, respectively.....60

Figure 22: Optical microscope image a micro-crack in a (PAH/PAA)_{5.5} film. Compressive stress was released at the film crack and affected the film buckling morphology for ~15 μm.....61

Figure 23: Optical microscope and AFM images of a buckled PDAC/SPS films on PDMS substrates after thermal processing. The smooth wavelike morphology was observed again but now for a film that was not known to crosslink. (a) Optical microscope image of a (PDAC/SPS)₂₀ film. (b) – (d) tapping mode AFM images of 10, 20 and 40 bilayer PDAC/SPS films respectively.....63

Figure 24: Optical microscope image of the manually compressed (PDAC/SPS)₂₀ film. The average wavelength was found to be 3.26 μm.....65

Figure 25: Optical microscope and AFM images of a PAH (SPS/PDAC)_{19.5} film on PDMS with no plasma treatment before multilayer assembly. The amplitude of the waves was high because there was no SiO₂ layer to help absorb the compressive strain.....68

Figure 26: Optical microscope images of a (PAH/PAA)_{5.5} film on a topographically patterned PDMS substrate after thermal processing. The column diameter determines whether the buckled film was ordered ($d > \lambda$) or randomly oriented ($d < \lambda$). The scale bar is valid to all images.....69

Figure 27: (a) Schematic illustration of the composite nanoparticle/polyelectrolyte film, (PDAC/SiO₂ (PDAC/SPS)₄)₄, film before and after thermal processing. (b) AFM image of the film after thermal processing. The addition of nanoparticles alleviates the compressive stress and prevents buckling.....71

Figure 28: Optical microscope images of the composite nanoparticle/polyelectrolyte film, (PDAC/SiO₂ (PDAC/SPS)₄)₄ (a) before and (b) after thermal processing. The addition of nanoparticles alleviates the compressive stress and prevents buckling.....72

Images in this dissertation appear in color.

List of Abbreviations

6-CF	6-carboxyfluorescein
AFM	Atomic force microscopy
DI	Deionized
DMAB	Dimethylamine borane
DA	Directed assembly
EDS	Energy dispersive x-ray spectroscopy
ELD	Electroless deposition
GIC	Graphite intercalate compounds
HCl	Hydrochloric acid
LbL	Layer-by-layer
μ CP	Microcontact printing
M	mol/L
PAA	Poly(acrylic acid)
PAH	Poly(allylamine hydrochloride)
PAMAM	Poly(amidoamine)
PDAC	Poly(diallyldimethylammonium chloride)
PDMS	Poly(dimethylsiloxane)
PEM	Polyelectrolyte multilayers
pK_a	Acidic dissociation constant
QCM	Quartz crystal microbalance
RFID	Radio frequency identification
RMS	Root mean square
SAM	Self-assembled monolayer
SEM	Scanning electron microscope
SPS	Sulfonated poly(styrene)
TEM	Transmission electron microscope
xGnP TM	Exfoliated graphite nanoplatelets

to
an
dis
en
intr
pol
film
bec
allo
diffe
part
opp
inter
proc
The
as c
poly
prop
Th
and
solu

Chapter 1: Introduction to Polyelectrolyte Multilayers

The development of functional thin films for a variety of applications has been a topic of interest for many researchers over recent decades. The investigation and study of these films has been performed by scientists from a variety of disciplines including chemistry, physics, electrical engineering, chemical engineering and materials science. One simple method of forming films was introduced by Decher in 1991.¹ Decher showed that oppositely charged polymers in solution can be alternately adsorbed one layer at a time to form thin films on charged substrates. This ionic layer-by-layer (LbL) assembly has become quite ubiquitous because it is an inexpensive and versatile method that allows nanometer scale control of film thickness on planar and 3D surfaces. The different types of substrates include glass, metal oxides, silicon wafers, colloidal particles and both stiff and flexible plastics. Films formed by the LbL build up of oppositely charged poly-ionic polymers or polyelectrolytes using electrostatic interactions are called polyelectrolyte multilayers (PEM). A schematic of the process along with common polyelectrolyte structures are shown in **Figure 1**. The technique of LbL assembly has been extended to different interactions such as covalent or hydrogen bonding and van der waals interactions.² The ultra thin polyelectrolyte layers add chemical functionality and change the surface properties.

The physical structure of the film can be controlled by the formation process³⁻⁷ and by the deposition conditions during assembly (e.g., ionic strength^{3, 8-10} and solution pH^{11, 12}). Adding a simple drying step after each polymer deposition step

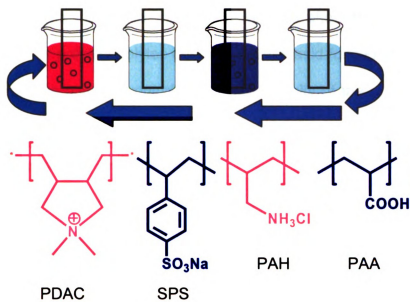


Figure 1: Schematic illustration of LbL assembly and chemical structure for common strong (PDAC and SPS) and weak (PAH and PAA) polyelectrolytes.

can change the final thickness of the fabricated films.³ Additionally, spraying the polyelectrolyte solutions onto the substrate significantly reduces the processing time and can increase the surface coverage of the first few deposited layers.^{4, 5} LbL assembly using spin-coating has also been demonstrated as another method to create PEM.^{6, 7} The resulting film structure is dependent on the polyelectrolyte concentration and spin rate, and can be utilized to reduce the surface roughness of the PEM film. The ionic strength or amount of dissolved salts in the polymer solution can affect the thickness of an adsorbed polyelectrolyte layer.^{3, 8-10} Increasing the ionic content of the assembly solution will cause more charge screening to occur. This yields a more coiled or loopy conformation of the polymer since consecutive charges along the polymer chain are no longer electrostatically repelled by one other. The more loop-rich morphology results in a larger thickness when the polymer is adsorbed onto the

surface. The pH of the assembly solution will also affect the thickness of the adsorbed layer for polyelectrolytes containing weak acid functionalities.^{11, 12} The solution pH can be used to control the charge density of the polymer chains in solution. For example weak polyelectrolytes containing amine functionalities will have a positive charge when the pH is below the acidic dissociation constant (pK_a). The polyelectrolyte will have a high charge density along the polymer backbone and will adsorb to a surface in an elongated conformation. When the solution pH is near or greater than the pK_a the polymer chain is coiled due to a decrease in the charge density along the polymer chain. This will cause a more loop-rich conformation and greater thickness for an adsorbed layer. Rubner and coworkers¹² have used weak polyelectrolytes to create three different film morphologies. The first is a loop-rich PEM film with two low charge density polyelectrolytes. The second conformation is elongated using two densely charged polyelectrolytes. The third is an intermediate using one low charge density and one densely charged polyelectrolyte. These different film architectures have been used for numerous applications including controlling cell adhesion to a surface.¹³ For the low charge density polyelectrolyte system an acid treatment step after film formation creates a porous film morphology.^{14, 15} The size of the pores can be controlled by the pH of the solution. The morphology of these films can be cyclically changed from a non-porous to a porous state and back, by alternately immersing the films in solutions of moderate and low pH. Furthermore, ionic strength and pH have been used to

con

typ

S

12.1

em

one

will

laye

cou

Du

into

inco

appl

wrink

antir

surfa

have

or cl

other

elect

inorg

mater

temp

control the selective adsorption of PEM onto surfaces containing two different types of functional groups on the surface.^{3, 16}

Surface properties such as surface wetting (i.e. contact angle) can be altered.^{11, 12, 17} The water contact angle can be controlled by the type of polyelectrolytes employed for LbL. Typically the contact angle alternates between two values, one angle corresponding to each polyelectrolyte. Additionally, the contact angle will vary slightly for each polyelectrolyte due to the thickness of the last adsorbed layer, the amount of interpenetration and contact angle associated with the counter polyelectrolyte in the PEM.

Due to the simplicity of LbL, diverse types of materials have been incorporated into the film as single or multiple layers. Depending on how the materials are incorporated they can have vast differences in the resulting properties or applications. Silica or polystyrene particles have been used to prevent wrinkling¹⁸ and create superhydrophilic,¹⁹ superhydrophobic,^{20, 21} reflective²² or antireflective^{23, 24} surfaces. PEM can be used to densely adsorb proteins to a surface²⁵ or prevent proteins from adsorbing to a surface.²⁶ Additionally, proteins have also been used in LbL assembly to create biosensors.²⁷ Carbon nanotubes or clays have been used to strengthen PEM composite films.^{28, 29} Numerous other types of functional materials including lipid bilayers, electro-optic, electroluminescent and conductive materials, dielectric layers, and organic or inorganic nanoparticles have been incorporated into PEM films.³⁰ When these materials are used in LbL assembly and are combined with inexpensive templating or patterning techniques, 3D films with nanometer scale dimensions

ca
co
all
ap
and
S
lith
whi
Add
ass
stud

can be fabricated for useful applications. The deposition of PEM onto a planar or colloidal sacrificial substrate followed by the dissolution the substrate, has allowed for the creation of free standing films or membranes.³¹ These films have applications in thermal mechanical sensing, controlled release, optical detection and drug release.

Since virtually any surface can be coated with PEM, PEM combined with soft-lithographic patterning techniques enable the fabrication of conductive patterns which can be created on inexpensive, flexible and non-planer substrates. Additionally, since the incorporation of functional materials during the LbL assembly of PEM is extremely simple, PEM are excellent candidates for the study of the mechanical properties of the composite films.

Chapter 2: A Versatile Approach to Selective and Inexpensive Copper Patterns Using Polyelectrolyte Multilayer Coatings

Introduction

Flexible substrates and inexpensive metal patterning techniques with high selectivity have been the focus of current research in displays, radio frequency identification (RFID) transponders, sensors and other nano- and microelectronic device fabrication.³²⁻³⁴ Recently, many techniques have been developed to pattern metals on surfaces.³⁵⁻⁴¹ Since most of these techniques are surface-specific, when the substrates are changed these techniques fail to function properly. A more general and versatile approach to patterning metals is demanded for current and rapidly changing microelectronic applications. Photolithography based top-down methods are the standard industrial patterning technique in microelectronics. However, this process is an expensive step in device fabrication, limits the functionality of substrates and other materials, and has an inability to work with curved substrates or the complex 3D structures needed for new electronic devices.^{33, 42, 43} Microcontact printing (μ CP), a soft lithographic patterning technique, combined with PEM coatings offers a multitude of cost-effective routes for creating functional three dimensional structures on plastic and other flexible substrates.³⁰ Electroless deposition (ELD) is a convenient, inexpensive metal plating technique that works on nano- or micrometer sized objects and can be used to selectively plate metal onto 2D and 3D structures.⁴⁴⁻⁴⁶ The combination of PEM coatings, μ CP, and ELD can provide a more economical approach for microelectronic fabrication on a wider range of substrates including plastic and flexible substrates.

PEM coatings can be used to create platforms with surface properties which are independent of the substrate they are formed on.^{1, 30} μ CP is excellent for high throughput large area patterning with micron and submicron feature sizes. Stamps for this process are created by curing poly(dimethylsiloxane) (PDMS) onto a master patterned by photolithography. By using μ CP, numerous devices can be fabricated from a single photolithographic step; however devices produced solely from photolithography require the expensive photolithographic step to be repeated once per device. PDMS stamps were first used to create patterns of thiols on gold,⁴⁷ and silanes on silica.⁴⁸ Many other functional materials including m-d-peg acid,⁴⁹ polymers,^{50, 51} polyelectrolyte aggregates⁵² and dendrimers^{53, 54} have been patterned onto PEM coated substrates. LbL assembly on PDMS stamps and subsequent μ CP was used to create 3D structures of PEM and bionanocomposite arrays with excellent selectivity.⁵⁵⁻⁵⁸

μ CP and ELD have been used together to create selective metal patterns which are less expensive to produce than patterns created by conventional photolithography.³⁵⁻⁴¹ By using μ CP and ELD, numerous devices can be fabricated from a single photolithographic step; however devices produced solely from photolithography require the expensive photolithographic step to be repeated once per device. Metal patterns have been created from the electroless deposition of copper, silver, gold, nickel and cobalt patterns, typically on silica substrates with palladium based catalysts. ELD catalysts do not strongly adhere to the substrate so an adhesion layer is required. To overcome this obstacle, a silane self-assembled monolayer (SAM) has been used as the

adhesive layer.^{36, 37, 39} Substrates with patterned catalyst are created by directly stamping the catalyst or via an indirect method such as patterning the adhesion layer. Other ELD adhesion layers include phosphine-phosphonic acids,³⁵ titanium³⁸ and poly(amidoamine) dendrimers.^{40, 41} While these adhesion layers are effective, they are limited because they form substrate specific bonds that are not interchangeable like electrostatic charges. Additionally our method is more versatile because the chemical functional groups of the polyelectrolyte adhesion layer can be changed and other materials can easily be added to the multilayers optimize the system.

LbL assembly of PEM has been combined with ELD to make selective nickel patterns on glass and plastic substrates coated with PEM.^{59, 60} This method uses PEM as the adhesion layer between the substrate and the deposited nickel. Ink-jet printing was used to pattern a polyelectrolyte ink onto a PEM surface resulting in plus/minus patterned regions. Then, directed self-assembly was used to selectively adsorb an ionic palladium catalyst onto the plus/minus patterned surface using electrostatic interactions. This approach is limited by the ink-jet printing resolution which is at best 20 μm ,⁴² while μCP is reported to have a much finer resolution, 30 nm.⁴³ In addition, the directed self-assembly of charged catalysts onto functionally patterned surfaces often led to poor selectivity of metal patterns on surfaces.⁴⁴

We present a new process for creating versatile and selective copper patterns by combining PEM coatings, μCP , and ELD. For the first time μCP was used to pattern a charged palladium catalyst onto oppositely charged PEM coated

substrates. PEM, unlike silanes and thiols, can be stably coated onto virtually any substrate including hydrophobic polymer surfaces.³⁰ This results in a highly selective electrostatically bound charged palladium ion complex on the PEM coated substrates. The substrate was then placed into an ELD bath where copper selectively plated only at the catalyzed regions. Our system which involves PEM as the stable adhesion layer is more versatile, economical and works over a larger range of substrates than previous approaches. The combination of PEM and μ CP allows the control of 3D features on the micron and submicron scale. Using our process it was possible to create stable and selective copper patterns with nanometer dimensions on flexible substrates, which can result in lower fabrication costs to produce flexible display electronic circuits, sensors, RFID transponders, and other nano- or microelectronic devices.

Experimental Details

Materials: Poly(diallyldimethylammonium chloride) (PDAC, Mw ~ 70,000), sulfonated poly(styrene), sodium salt (SPS, Mw ~ 150,000), dimethylamine borane (DMAB), 2,2' dipyridyl, and 16-mercaptohexadecanoic acid were purchased from Sigma-Aldrich (Milwaukee, WI). Triethanolamine and 1,5,8,12-tetraazadodecane were purchased from Fisher Scientific (Pittsburgh, PA). The palladium catalyst, $\text{Na}_2[\text{PdCl}_4]$, was purchased from Strem Chemicals (Newburyport, MA). Cupric sulfate was purchased from J.T. Baker (Phillipsburg, NJ). A Sylgard 184 elastomer kit was obtained from Dow Corning (Midland, MI) to create poly(dimethylsiloxane) (PDMS) stamps. Deionized (DI) water from a

Barnstead Nanopure Diamond (Barnstead International, Dubuque, IA, resistivity >18.2 M Ω -cm) purification system was used exclusively for all experiments.

Substrate Preparation: Glass microscope slides (Corning Glass Works, Corning, New York) were sonicated with a Branson ultrasonic cleaner (Branson Ultrasonics Corporation, Danbury, CT) for 20 minutes in an Alconox (Alconox Inc., New York, NY) solution followed by 10 minutes of sonication in water. The slides were then blown dry with nitrogen and plasma cleaned (Harrick Scientific Corporation, Broadway Ossining, NY) with oxygen at \sim .125 Torr for 10 minutes. Before use, polystyrene microscope slides (Nalge Nunc International, Rochester NY) and flexible polyester transparency films (3M, St. Paul, MN) were plasma treated under the same conditions for 10 minutes. A Carl Zeiss slide stainer (Richard-Allan Scientific, Kalamazoo, MI) connected to a computer and equipped with a custom-designed ultra sonication bath (Advanced Sonic Processing, Oxford, CT) was used to mechanically coat the substrates with PEM.⁶¹ Positively charged PDAC and negatively charged SPS were deposited onto the slides from 0.02 mol/L (moles per liter, M) solutions containing 0.1 M NaCl. The samples were dipped into the polymer solution for 20 minutes followed by washing. One layer of PDAC followed by a layer of SPS was used to create a single bilayer. Typically a PDAC topped 10.5 bilayer film, denoted as (PDAC/SPS)_{10.5} was used when a positive surface was desired.

Microcontact Printing: A Sylgard 184 elastomer kit (Dow Corning, Midland, MI) was used to create PDMS stamps which were used for μ CP.⁴⁷ These stamps were created by pouring the prepolymer and initiator (10:1 mass ratio) on

top of a fluorosilane treated patterned silicon master cured in an oven overnight at 60 °C. The masters were prepared in the Microsystems Technology Lab at Massachusetts Institute of Technology or Keck Microfabrication Facility at Michigan State University and consisted of lines with widths from 1.25 to 10 μm . The fluorosilane treatment allowed for easy separation between the master and the cured PDMS. The stamps were cut to size and washed with soap and water before use. Before stamping, the PDMS stamps were oxygen plasma cleaned for four minutes to make their surface hydrophilic. The PDMS stamps were soaked for 20 minutes in a freshly prepared 5 mM aqueous solution of the palladium catalyst. The stamps were removed from the ink solution, blown dry using nitrogen and brought into conformal contact with the PEM surface for five minutes. Then they were removed and the patterned samples were rinsed with flowing DI water. Since the catalyst ink solution has an unadjusted pH of ~ 3.0 , the rinse water pH was lowered to 3.0 by adding a small amount of 1.0 M hydrochloric acid (HCl).

Electroless Deposition Bath: Copper was selectively plated onto the previously deposited catalyst regions using a previously optimized electroless bath.⁶² The electroless bath contained 0.032 M cupric sulfate, 0.040 M 1,5,8,12-tetraazadodecane, 0.300 M triethanolamine, 0.067 M dimethylamine borane and 300 mg/mL 2,2' dipyridyl in DI water. The copper bath was used at a temperature of 50 ± 2.0 °C and the pH was adjusted to 9.0 ± 0.1 by adding a few drops of 1.0 M HCl.

Colloidal Adsorption: To show that the unpatterned surface was still functional (i.e. charged) and available for further modification or processing after metal deposition, colloidal particles were deposited onto the PDAC regions of the surface. A 0.5 wt % colloidal solution of 4 μ m carboxylated polystyrene particles (Interfacial Dynamics Corp., Portland, OR) was gently dropped on the surface of a copper patterned glass slide and incubated for three hours. The particle coated substrates were then washed carefully with DI water and blown dry using nitrogen.

Quartz Crystal Microbalance Crystal Preparation: Gold coated quartz crystal microbalance (QCM) crystals (5 MHz, Maxtek, Inc., Santa Fe Springs, CA) were cleaned in fresh piranha solution (7:3 concentrated sulfuric acid; 30% hydrogen peroxide) for 20 seconds, rinsed with copious amount of water and blown dry with nitrogen. The crystals were then immersed into an ethanol solution containing 5 mM 16-mercaptohexadecanoic acid (Aldrich) for 30 minutes, copiously rinsed with ethanol and blown dry with nitrogen. Then multilayers, (PDAC/SPS)_{10.5}, were deposited onto the QCM crystal as described previously. A 30 second immersion into a freshly prepared 5 mM aqueous palladium catalyst solution followed by a DI water rinse was used to catalyze the crystals before electroless deposition.

Characterization: Optical microscope images were taken using a Nikon Eclipse ME600 microscope equipped with a digital camera. Atomic force microscope (AFM) images were collected in tapping mode using a Nanoscope IV multimode scope from Digital Instruments. An environmental scanning electron

microscope (SEM, model 2020, Electro Scan) equipped with a LaB₆ filament and operated at 20 kV with a water vapor environment in the sample chamber was used to obtain SEM images. Energy dispersive x-ray spectroscopy (EDS) spectra were obtained using a Link ISIS system (Oxford Instruments). Metal plating rates were measured using a research QCM (Maxtek, Inc.) and accompanying computer software.

Results and Discussion

Figure 2 shows the overall scheme of the fabrication process. To demonstrate the versatile and selective metal patterning process on virtually any surface type, three representative substrates, hydrophilic glass, hydrophobic polystyrene and flexible polyester transparency film substrates were selected. With the addition

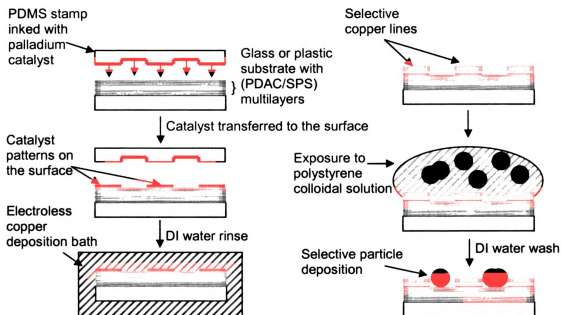


Figure 2: Schematic of the overall fabrication process to create selective copper patterns on PEM coated substrates followed by colloidal deposition.

of only a few polyelectrolyte bilayers the surface properties of a substrate can be completely changed to have either a positive or negative charge.³⁰ With this in mind, 10.5 bilayers of positively charged PDAC and negatively charged SPS, (PDAC/SPS)_{10.5}, were fabricated on glass and plastic substrates to create an outer surface with properties that are independent from the original substrate. These PEM have a positively charged surface and a total thickness of ~30nm.⁴⁹ An oxygen plasma treated PDMS stamp was soaked in a freshly prepared aqueous 5 mM ink solution that contained negatively charged palladium, and has a natural pH of ~3.0. After soaking, the stamps were blown dry with nitrogen and placed in conformal contact with the positively charged surface of the PEM. While in contact with the surface, the negatively charged palladium ions transferred to the positively charged surface via electrostatic interactions. After the stamp was removed, the patterned PEM surface was rinsed with DI water at a pH of ~3.0 to remove the excess catalyst. After rinsing, the substrates contained alternating regions of positively charged PDAC and negatively charged palladium catalyst complexes. These catalyst patterned substrates were then placed in an electroless copper bath. This bath which was previously optimized has excellent selectivity and operates at a lower pH than the traditional formaldehyde based electroless baths.⁶² The copper bath was heated to 50 ± 2°C and then DMAB was added to initiate the chemical reaction. The solution pH was reduced to 9.0 ± 0.1 using a small amount of 1.0 M HCl. The catalyzed substrates were placed into the electroless copper bath where DMAB reduced the positive copper ions to zerovalent metallic copper which selectively adsorbed

onto the substrate in the regions of the surface where the palladium catalyst was present. Copper deposition did not occur at the uncatalyzed regions of the surface, so the positively charged PDAC regions of the surface were copper free.

Figure 3 shows optical micrograph images of the selective copper patterns. Reflected light optical microscope images of copper patterns on PEM coated glass and polystyrene substrates are shown in **Figure 3a-c**. Plated copper was only found where the PDMS stamp was in contact with the positively charged polymer. It was possible to create highly selective results (i.e., nearly 100 % selectivity) over areas as large as the entire stamp ($\sim 1 \text{ cm}^2$). Unlike our direct catalyst stamping on PEM coated substrates, the directed assembly of catalysts onto plus/minus (polycation/polyanion) micropatterned regions^{50, 51} resulted in

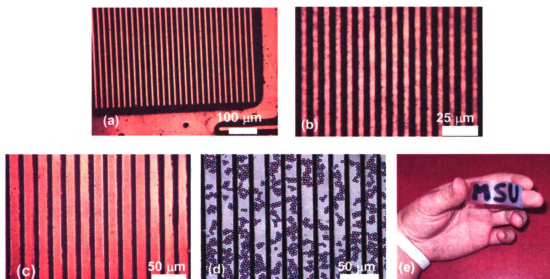


Figure 3: Reflected light optical micrographs of selective copper lines on PEM coated substrates. Parts (a) and (b) have glass substrates while (c) is on a polystyrene substrate. (d) Transmitted light optical micrograph of polystyrene particles deposited on the active unpatterned regions of the PEM surface next to the black copper lines. (e) A PEM coated flexible transparency film substrate with electroless copper patterns which are $\sim 30 \text{ nm}$ thick.

less selective metal patterns.⁵⁴ We believe that this is because polycations and polyanions are integrated through the multilayers so that 'plus' and 'minus' patterned regions are not exclusively homogeneous at the molecular level (see Chapter 3 for more discussion on this topic) on which the small charged catalysts cannot be completely directed to the oppositely charged regions. Only direct catalyst stamping onto PEM can generate confined catalyst nano and micropatterns, which result in 100% selective metal patterns. In addition, the positively charged unpatterned PDAC surface was still active and could be modified further. To demonstrate this we deposited negatively charged polystyrene particles onto the unpatterned regions of the surface, **Figure 3d**. Previously our group has shown that complete surface coverage of the particle monolayer is not expected from a simple drop coating.²³ **Figure 3e** shows an electroless copper pattern on a polyester transparency film that was coated with a PEM adhesion layer. The palladium catalyst was patterned on the surface using a cotton-tipped swab. This image demonstrates that flexible polyester transparency films can be patterned using our technique.

AFM was performed to further analyze the sample topography. The AFM images in **Figure 4** again show that copper deposition scarcely occurs outside the patterned regions on the PEM surface. The sample **Figure 4a** has an average copper thickness of $107.6 \pm 4.3\text{nm}$. The surface roughness of the deposited copper lines is 20 nm. **Figure 4c** shows a sample that was stamped using two different stamps with a 90° separation in orientation and before

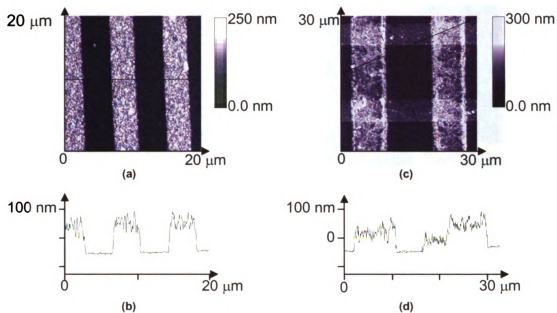


Figure 4: AFM images of (a) a $20\ \mu\text{m} \times 20\ \mu\text{m}$ image of selective copper patterns and (b) a $30\ \mu\text{m} \times 30\ \mu\text{m}$ image of multilevel structure created by stamping a substrate twice before electroless deposition.

immersion into a copper bath. This illustrates that complex 3D metal structures can be fabricated on PEM surfaces.

Figure 5 shows an SEM image of the selective copper patterns. EDS analysis of the sample confirms that copper was being deposited in linear patterns on the PEM surface. More importantly, the second spectrum shows that there was no detectable copper present on the polymer surface between the copper lines. The calcium peak was kept so relative peak heights between the copper lines and polymer surface could be compared. All other detected elements were due to the PEM and the glass substrate.

A QCM was used to study the kinetics of ELD on unpatterned homogeneously catalyzed or uncatalyzed surfaces. A carboxylic acid terminated thiol was used to create a SAM on the gold coated quartz crystals. This results in a negatively

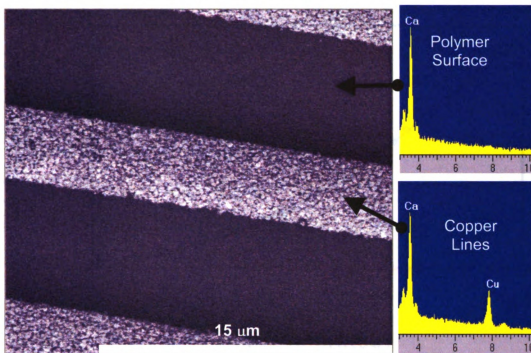


Figure 5: SEM image selectively plated copper lines on PEM. The EDS spectra shown are for the copper lines and the unpatterned polymer surface. The calcium peak was left to show the relative size of the copper peak.

charged outer surface. (PDAC/SPS)_{10.5} bilayers were deposited on the thiol to create uncatalyzed QCM crystals. The crystals were catalyzed by immersion into an aqueous palladium catalyst solution followed by rinsing with DI water (pH ~3.0). The QCM crystal and the copper bath were simultaneously heated to 50°C. The copper bath was then activated and the pH was adjusted. The warm QCM crystal was placed into the activated copper bath. The change in copper thickness was calculated from the change in frequency of the QCM crystal using the QCM computer software. The QCM results are shown for a catalyzed (blue squares) and uncatalyzed (red triangles) PDAC surface in **Figure 6**. The different plating rates shown in the plot verify the high selectivity of the electroless copper bath. Copper uniformly plates on the catalyzed surface and

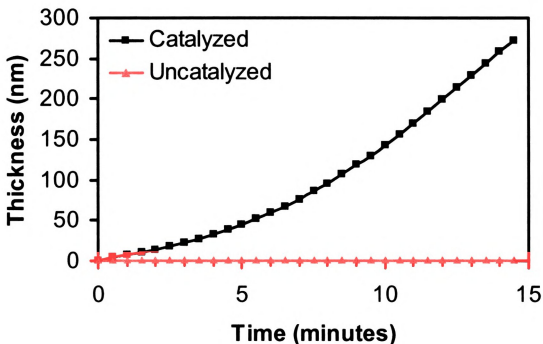


Figure 6: QCM results of copper thickness versus time for homogeneously catalyzed and uncatalyzed surfaces.

does not deposit on the uncatalyzed PDAC surface. The initial non-linear plating rate of the catalyzed sample is caused by the increasing area available for copper deposition. After seven minutes linear growth was observed with an average plating rate of 26.8 nm/min. This plating rate agrees well with the previously reported rate of 23.3 nm/min for the same copper bath under similar conditions.⁶²

We were able to create copper thicknesses of up to 300nm using only electroless deposition. Delamination of copper films thicker than 300 nm occurred due to the build up of internal stress in the ELD copper thin films. This problem may be solved using a combination of electrodeposition and thermal annealing. Electrodeposition of a second copper layer onto the ELD copper seed layer followed by thermal annealing will increase the total copper thickness,



re
c
C
I
be
co
pa
The
can
dis
with
PEM
struc

reduce the internal stress and increase the strength of adhesion between the copper layers.^{63, 64} Currently, we are working to resolve this issue.

Conclusion

In conclusion, a novel versatile process incorporating PEM, μ CP and ELD has been utilized to create copper patterns with excellent selectivity on top of PEM coated substrates. μ CP and ELD together reduce fabrication costs of metal patterns and structures compared to conventional photolithographic techniques. The ability of PEM to coat any surface³⁰ allows bendable plastic to be used and can reduce the cost of materials in future electronic devices such as bendable displays, sensors, and RFID transponders. The combination of LbL assembly with μ CP gives nanoscale control of the feature dimensions. The copper free PEM surface was still functional and can be modified to fabricate 3D metal structures or even patterns composed of two or more metals.

Chapter 3: Effects of Catalyst Introduction Methods Using PAMAM Dendrimers on Selective Electroless Nickel Deposition on Polyelectrolyte Multilayers

Introduction

A new direction for research in thin-film transistors, organic light-emitting diodes and other microelectronic devices is to find methods that will enable the fabrication of flexible devices.^{65, 66} As shown in Chapter 2 the combination of PEM coatings, μ CP and ELD can be used to create metal patterns on a variety of different substrates.⁶⁷ The LbL assembly of polyelectrolytes is an inexpensive method to create a surface with properties independent from the substrate (i.e. glass, metal oxides, silicon wafers, and both stiff and flexible plastics).¹ μ CP is a simple softlithographic approach to patterning which uses an elastomeric stamp to create patterns over large surface areas.⁴² This method is more advantageous than the current technique, photolithography, because it allows for the use of non-planar substrates and does not severely limit the types of materials that can be used. ELD is a nanoscale metal deposition technique which can selectively pattern three dimensional surfaces.^{44, 68}

μ CP and ELD have been combined to pattern of various types of metals.^{35-38, 69,}
⁷⁰ Silane self-assembled monolayers, titanium and polymers have been used as adhesion layers to attach the ELD catalysts to their substrates. However, all of these approaches use specific interactions between the adhesion layer and substrate which are not universal like electrostatic charges. If the substrate is changed, these other methods are ineffective. However using a PEM adhesion layer allows the substrate to be changed with out affecting the patterns.^{59, 60, 67}

Cage-like poly(amidoamine) (PAMAM) dendrimers which offer precise control of their nanoscale size have been patterned using μ CP.^{53, 71, 72} These dendrimers are more advantageous for patterning since they do not diffuse on the surface like lower molecular weight materials such as alkane thiols. The hollow dendrimer interiors can be used to store functional nanomaterials. Crooks and coworkers have shown that monodisperse nanoparticles can be created inside the PAMAM dendrimers.⁷³ The interiors of the dendrimers serve as binding groups for metal ions. Once the ions are encapsulated they are reduced to form nanoparticles. During the reduction step the dendrimers prevent the nanoparticles from aggregating into larger particles. These nanoparticles can be used as catalysts for hydrogenation and other types of reactions. Additionally, Bittner and coworkers have created micropatterns of PAMAM dendrimers and utilized them as adhesion layers for ELD.^{40, 41} Most ELD papers show how to create metal patterns; no research has investigated how different methods of introducing the catalyst to a surface affects the resulting metal patterns.

In this work we show for the first time how the method of catalyst introduction affects the resulting patterned electroless deposition. PEM films were fabricated and used as platforms for electroless nickel patterning. μ CP was used to pattern the palladium catalyst on the PEM platforms. After applying the catalyst, the samples were placed into an electroless bath. In the electroless bath, the initial nickel plating rate, nickel morphology and nickel pattern selectivity (i.e., relative amount of metal deposition in desired places versus undesired places) were all affected by the method of catalyst introduction. Also, the number of PEM

bilayers required to remove the substrate effect on nickel patterning was investigated.

Experimental Details

Materials: Fourth generation poly(amidoamine) (G4 PAMAM) dendrimers, nickel sulfate, sodium citrate and lactic acid, were purchased from Sigma-Aldrich (Milwaukee, WI). Fluorescein isothiocyanate (FITC) was purchased from Molecular Probes (Eugene, Oregon). PDAC, SPS, DMAB, 16-mercaptohexadecanoic acid, the palladium catalyst, PDMS and DI water were obtain as described in Chapter 2.

Substrate Preparation: As described in Chapter 2, glass microscope slides were sonicated and plasma cleaned before PEM assembly. PEM of positively charged PDAC and negatively charged SPS were deposited onto the microscope slides using a computer controlled mechanical slide stainer. Both polyelectrolyte concentrations were 0.02 M (based on the polymer repeat unit) and contained 0.1 M NaCl. A PDAC topped ten and a half bilayer film, denoted as (PDAC/SPS)_{10.5}, was used when a positive surface was desired. A SPS topped ten bilayer film, denoted as (PDAC/SPS)₁₀, was used when a negative surface was desired.

Stamp Preparation: PDMS stamps were fabricated by mixing the prepolymer and initiator and pouring the mixture onto the patterned silicon master. The stamps were then cured overnight in an oven at 60 °C. The patterns consisted of circular patterns with diameters ranging from 1.25 to 9.0 μm. Before use the stamps were oxygen plasma treated for 30s to render the surface hydrophilic. A

cotton-tipped swab was used to apply the different inks to the stamp surface before drying with nitrogen. Contact times with the appropriately charged surfaces were typically 20s.

Ink Preparation: Three different methods were used to introduce the palladium catalyst to PEM surfaces; direct catalyst stamping (Method 1), directed assembly (DA, Method 2) using PAMAM dendrimers and catalyst encapsulation (Method 3) and reduction to nanoparticles inside PAMAM dendrimers. These methods are summarized in **Table 1**. The inks used in each method were prepared as follows.

Table 1: Summary of the three different catalyst introduction methods

<i>name</i>	<i>PEM surface</i>	<i>ink</i>	<i>additional steps</i>
Method 1	direct catalyst stamping	PDAC Pd catalyst	none
Method 2	directed assembly	SPS G4 dendrimer	adsorb Pd ions
Method 3	dendrimer assembly	SPS Pd in G4 dendrimer	none

1) Direct catalyst stamping: A 50 mM solution of the palladium catalyst was directly stamped onto a PDAC surface and rinsed with pH ~3.0 water. Nitrogen was used to dry the samples.

2) Directed assembly: A 0.1 wt% solution of G4 PAMAM in DI water was stamped onto a SPS surface. The substrate was then immersed in a 5 mM palladium catalyst solution for 10s. The substrate was then washed with DI water. The patterned substrates were then immersed in a 5mM palladium

catalyst solution for 10s. The substrate was then washed in water with a pH of ~3.0 and dried with nitrogen.

PAMAM dendrimers were fluorescently labeled with FITC using a standard procedure.⁵³ FITC was dissolved in water and then added to aqueous solutions containing PAMAM dendrimers using a 1:1 molecular ratio. The dendrimer and dye solution was allowed to stand overnight with light agitation. The solution was then placed in dialysis tubing and dialyzed against DI water overnight.

3) Catalyst Encapsulation: The palladium catalyst ions were placed in the interiors of G4 PAMAM dendrimers and reduced to form dendrimer encapsulated nanoparticles following a previously established protocol published by Crooks and coworkers.⁷⁴ The pH of a 0.1 wt% G4 dendrimer solution in DI water was reduced to ~3.0 using 0.1M HCL. Then 563 μ L of 0.1 M $\text{Na}_2[\text{PdCl}_4]$ was slowly added to the dendrimer solution. This gives a dendrimer to Pd ion ration of 1:40. The sample is allowed to mix for 30 minutes before adding a 10 M excess (0.025 g) of DMAB to the solution which reduces the Pd ions to metal nanoparticles. The solution was then filtered to remove large agglomerates.

Electroless Nickel Deposition: The catalyst patterned slides were then placed in an electroless nickel deposition bath. The nickel bath contained 4.0 g nickel sulfate (Ni source), 2.0 g sodium citrate (complexant), 1.0 g lactic acid (buffer, complexant) and 0.2 g DMAB (reducing agent) in 100 mL of DI water. Before use, the pH of the nickel bath was adjusted to 6.5 ± 0.1 by adding small amounts of NaOH solution. Catalyst patterned substrates were placed into the electroless bath for plating times between 10 and 15 minutes.

Quartz Crystal Preparation: Gold coated quartz crystals were cleaned immersed in an ethanol solution containing 5 mM 16-mercaptohexadecanoic acid as described in Chapter 2. The negatively charged samples were then placed in the slide stainer where (PDAC/SPS)₁₀ or (PDAC/SPS)_{10.5} bilayer films were assembled on their surface as described above. To simulate Method 1, (PDAC/SPS)_{10.5} bilayer films were used. To simulate Methods 2 and 3, (PDAC/SPS)₁₀ bilayer films on quartz crystal microbalance (QCM) crystals were immersed in a 0.1 wt% G4 dendrimer solution for 20 minutes. For samples simulating Method 3 the 0.1 wt% G4 solution contained dendrimer encapsulated palladium nanoparticles. For activating the QCM crystals that simulated Methods 1 and 2, the crystals were immersed in an aqueous solution containing 5 mM palladium catalyst for 10s. The samples were then mounted in the crystal holder and placed in to an electroless nickel bath. The computer software was used to measure the change in resonance frequency of the crystals.

Characterization: Optical and fluorescence microscope images were obtained using a digital camera mounted on a Nikon Eclipse ME 600 or ME 400 respectively. A JEOL (Japanese Electro Optics Laboratories) 2200FS 200 kV field emission transmission electron microscope (TEM) was used to obtain images of samples on carbon coated copper grids. AFM, SEM, EDS and QCM data were obtained as described in the previous chapter.

Results and Discussion

Building on the combination of μ CP, ELD and PEM from our previous work,^{44, 67} we explored different ways to introduce the catalyst to PEM surfaces. Using

PAMAM dendrimers, we patterned the negatively charged palladium catalyst on the PEM surface using three different methods, as summarized in **Table 1**. **Figure 7** illustrates the three different patterning methods we utilized. After the

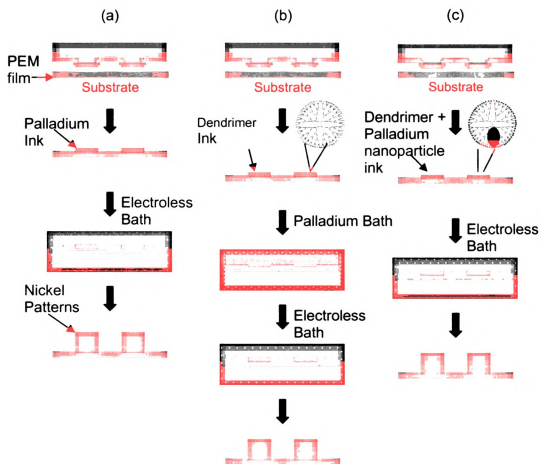


Figure 7: Process schematic for the three different methods. Methods 1-3 are depicted in parts a-c, respectively. Diagrams of the dendrimer and dendrimer-encapsulated nanoparticle structures are also included in parts b and c, respectively.

catalyst is patterned on the surface, the samples are placed in an electroless nickel bath that exclusively plated nickel in the regions where the palladium was

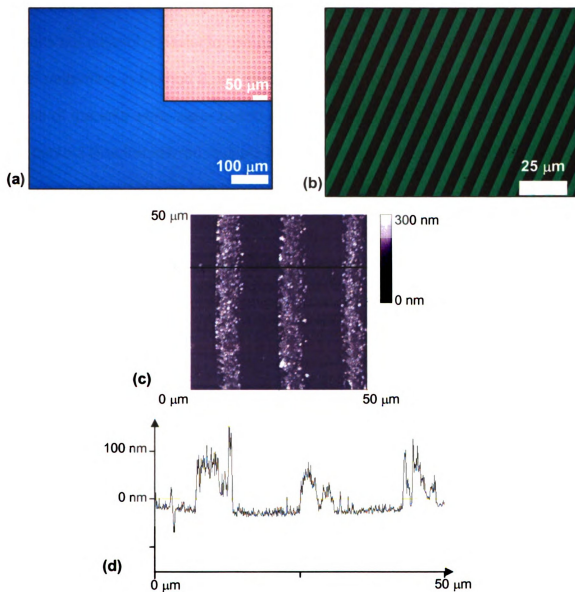
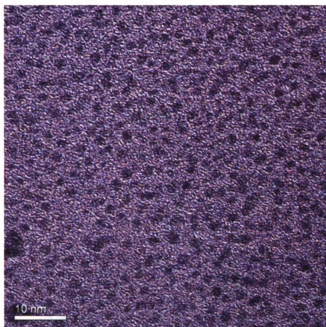


Figure 8: Optical microscope and AFM images of G4 PAMAM dendrimer patterns on PEM. (a) Phase contrast optical microscope images of two different pattern types with (large) and without (inset) a blue filter, (b) fluorescence microscope image of FITC-labeled PAMAM, (c) topographical AFM image of PAMAM patterns, and (d) sample line scan taken from the AFM image shown in (c).

present on the surface. **Figure 8** shows G4 PAMAM dendrimers patterned on a PS coated PEM surfaces before further modification. Dendrimer patterns could be created as large as the stamp ($\sim 1 \text{ cm}^2$). We used both ethanol and water as the solvent in our ink solution. We found that either solvent can create excellent patterns but ethanol is easier to use because it evaporates faster than water. For nickel patterning in Method 2, we used water as a solvent in the PAMAM ink so that all of the inks were water based and could be directly compared. Using a 20 s contact time transferred multiple layers of dendrimers to the surface. **Figure 8c** shows uniform patterns can be created before washing. The sample line scan in **Figure 8d** shows the dendrimers have an average height of $\sim 50 \text{ nm}$. This height of approximately 22 “monolayers” is consistent with thicknesses reported previously for μCPG4 PAMAM onto silicon wafers.⁷¹ After patterning, the samples were washed in water to remove the layer of weakly adsorbed dendrimers and left only a strongly adsorbed electrostatically bonded layer on the surface.⁵² AFM shows this strongly bound layer was typically 5-10 nm in thickness. The washed PAMAM surfaces were then used for nickel patterning.

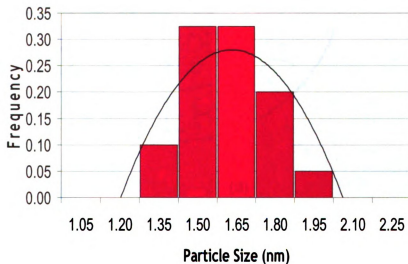
To test Method 3, palladium nanoparticles were created inside of the PAMAM dendrimers. The nanoparticle diameter was measured using TEM. **Figure 9** shows a TEM image of the dendrimer encapsulated nanoparticles and a graph of their size distribution. The dendrimers are not seen in the TEM image because they have little contrast against the carbon coating of the TEM grid. The average particle diameter was measured to be $1.6 \pm 0.2 \text{ nm}$. This is consistent with previously reported values for nanoparticles created using a 40:1 ion to

dendrimer ratio.^{74,75} These dendrimer encapsulated nanoparticle solutions were then used as inks for electroless nickel patterning.



(a)

Size Distribution



(b)

Figure 9: (a) TEM image of palladium nanoparticles fabricated in fourth generation PAMAM dendrimers. (b) Size distribution of the palladium nanoparticles.

Oxygen plasma treated PDMS stamps were used to transfer the ink to the appropriately charged surface (see **Table 1**). After patterning, samples were washed with DI water to remove the excess ink that was not electrostatically bound to the surface. In Method 2, after stamping, the samples were dipped into a 5 mM palladium solution where the negatively charged palladium ions adsorbed onto the positively charged PAMAM dendrimers. For all three methods, after the catalyst was patterned, the samples were placed into an electroless nickel solution. In the ELD, bath nickel was selectively plated where the

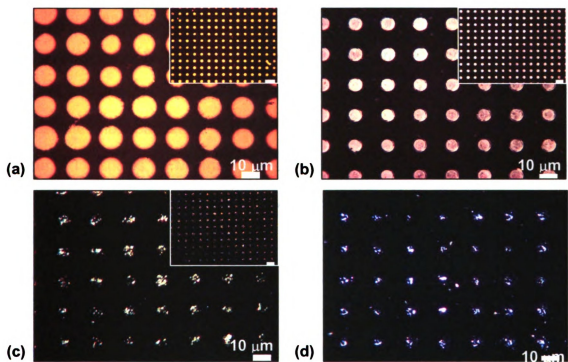


Figure 10: Optical microscope images of electroless-deposited nickel patterns. (a) and (b) Bright-field images of direct catalyst stamping (method 1) and DA (method 2) respectively. (c) Dark-field images of dendrimer-encapsulated nanoparticles (method 3). The insets show a larger sample area and have a 20 μm scale bar. (d) Dark-field microscope image of electroless-deposited nickel patterns created by μCP ions encapsulated in dendrimers. The ions were not reduced to nanoparticles before stamping.

palladium catalyst was found on the surface. **Figure 10** shows the resulting optical microscope images. All three methods successfully created nickel patterns on the PEM surfaces. The morphology produced by Method 3 is noticeably different than the morphology observed from Methods 1 and 2. This aggregated morphology of nickel was caused by the cage-like dendrimers which attached to the surface of the palladium nanoparticles and decreased the amount of active surface available for electroless deposition. This smaller active surface prevented nickel ions in the electroless bath from depositing and being reduced on the palladium nanoparticle surface as rapidly in Methods 1 and 2. We also created samples which contained dendrimer encapsulated palladium ions inside the dendrimers by leaving out the reduction step in ink preparation. These samples, shown in **Figure 10d**, display the same morphology as the dendrimer encapsulated nanoparticles.

Figure 11 shows AFM images produced by the three different methods. **Figure 11c**, the AFM image from Method 3, again shows the aggregated morphology caused by encapsulation of the catalyst. The small amounts of exposed nanoparticles slowly grow in the electroless bath. As they become larger they coalesce into one larger piece of nickel but still have a morphology of aggregated clusters. Method 1 produced a higher selectivity than Method 2. This is because in Method 2 the DA of catalyst molecules onto the plus/minus micropatterned surfaces resulted in less selective nickel patterns. We believe that this occurred because the surface was not completely homogeneous. The inhomogeneous surface is created by the interpenetration between consecutive

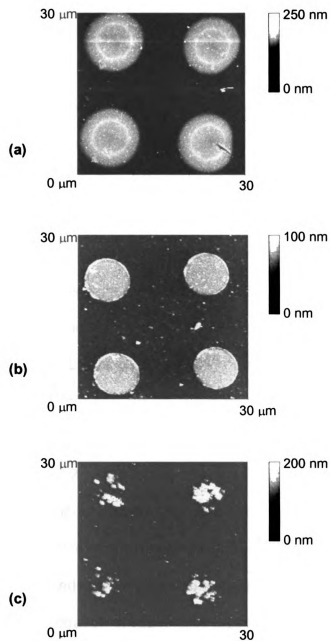


Figure 11: AFM images of nickel patterns using methods 1 (a), 2 (b), and 3 (c).

polyelectrolyte layers.¹ This means that the multilayers were not exclusively 'plus' or 'minus.' Instead, there were small domains on the PEM surface where

the tiny negatively charged catalyst molecules could find positively charged places on the unpatterned regions of a SPS surface. Only the direct catalyst stamping used in Method 1 can create 100% selectivity. When comparing samples produced by Methods 2 and 3, we observed that the encapsulation of the catalyst into the interior of the dendrimer inhibited and confined the nickel deposition. To produce the same pattern height as Methods 1 and 2, dendrimer encapsulated catalyst patterns required longer times in the ELD bath.

Since they are more appealing for practical applications, SEM was used to further analyze the samples from Methods 1 and 2. **Figure 12** shows that the direct catalyst stamping method had a slightly better selectivity than the DA method. This is verified by the EDS spectra obtained from the two different samples. When the polymer spectra were compared with the nickel spectra of the same sample, the difference in the amount of nickel detected is much greater for Method 1 than Method 2. So a larger difference in the nickel peaks means a larger difference in the amount of nickel deposited on the unpatterned regions.

The lower selectivity of Method 2 as compared to Method 1, suggests the last layer of polyelectrolyte adsorbed is not the only layer which affects nickel deposition. The interpenetration of subsurface layers of polyelectrolyte may have an effect on the selectivity of the palladium ion and subsequent nickel deposition. Additionally, Decher and coworkers have shown that during the initial buildup of PEM there exists a zone in which the substrate affects the PEM formation.⁹ This zone is ~4 bilayers in thickness. We investigated the effect of the number of bilayers on the patterning of nickel using Method 2. Glass slides were coated

with 0, 1, 3, and 5 bilayers of PDAC/SPS. These films have a thickness ranging from <5 to 18 nm.³ Nickel patterns were then created using directed assembly. The resulting optical micrographs are shown in **Figure 13**. The images show that as the number of bilayers increases the selectivity and quality of the patterns increases. With only one bilayer the quality of the patterns and the selectivity are

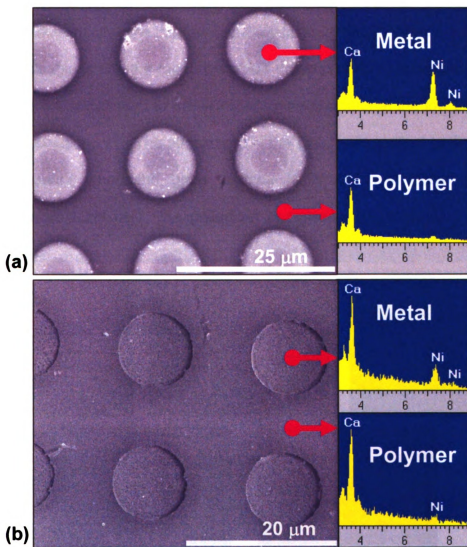


Figure 12: SEM images of patterned nickel samples created by methods 1 (a) and 2 (b). These images are accompanied with EDS spectra for the metal and polymer surfaces.

low. At three bilayers the selectivity is good however; the patterning is still not complete. The five bilayer samples show an increase in the quality of the patterns. At more than five bilayers the patterning quality and selectivity have reached the same level as seen for the ten bilayer slides which are normally used for Method 2. Interestingly, when the negatively charged catalyst was exposed to the PAMAM patterned glass slide (0 PEM bilayers), the catalyst deposited preferentially onto the glass surface instead of the PAMAM dendrimers. We speculate this is due the rapid hydrolysis of the palladium catalyst in solution and subsequent attachment to the $-OH$ terminated surface at the low pH (~ 3) of our catalyst solution.^{76, 77} The attachment of the hydrolysis product to the surface is not observed when the glass surface is coated with polyelectrolytes. Furthermore at a pH of 3, the palladium complexes are competing with the

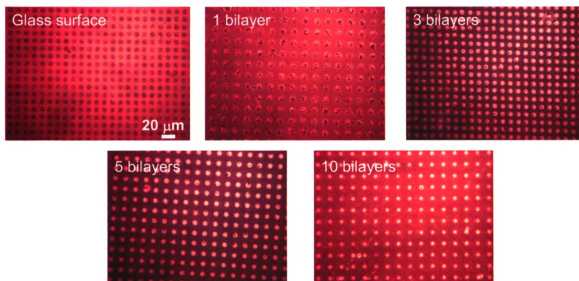


Figure 13: Optical microscope images of samples created using DA (method 2). The number of bilayers affects the selectivity and quality of the deposited nickel patterns. The scale bar is valid for all images.

protons to interact with the primary and tertiary amines of the PAMAM dendrimer. This causes the primary amines to become inert and the tertiary amines to react slowly to form covalent bonds with the palladium complexes.⁷⁴ Since we use a 10s immersion time, the palladium only electrostatically interacts with the dendrimers. Nickel deposition will occur as a result of these two processes. However **Figure 13** suggests that hydrolysis deposits more palladium to the surface which causes more nickel to be observed on the glass surface than the PAMAM regions.

QCM was used to compare the plating rates of the three different catalyst introduction methods using a homogeneous surface. Gold coated quartz crystals were coated with a –COOH terminated self-assembled monolayer (SAM). This SAM created a negatively charged surface which was then used as a starting point for PEM buildup. To simulate Method 1, (PDAC/SPS)_{10.5} bilayer coated crystals with an outer PDAC surface were catalyzed with palladium and placed in an electroless bath. Method 2 was simulated by starting with a (PDAC/SPS)₁₀ bilayer coated crystal and adsorbing a layer of PAMAM dendrimers before the adsorption of the negatively charged catalyst. Additionally, a (PDAC/SPS)₁₀ bilayer coated crystal was used to simulate the unpatterned SPS regions on the surface. Dendrimer encapsulated nanoparticles were adsorbed onto the surface of a (PDAC/SPS)₁₀ bilayer coated crystal to simulate Method 3. The resulting kinetic data are shown in **Figure 14**. The nickel growth rate for all three methods has two general zones; an initial growth zone and then a linear growth zone. The plating rates for Methods 1 (PDAC surface) and 2 (PAMAM surface) are

virtually the same. However, Method 3 (PAMAM and nanoparticle surface) shows a slower initial growth rate which causes the use of a longer time before a linear growth rate is observed. This decrease in the initial growth rate is caused by the cage like PAMAM dendrimers covering the surface of the palladium nanoparticle catalyst which prevents the nickel deposition from occurring as freely as in Method 1 or 2. Once the surface is completely coated with metal, then a linear growth rate of ~ 4.7 nm/min is observed for all three methods. To confirm that a catalyst is required for the electroless deposition, uncatalyzed surfaces of both SPS and PDAC were placed in an electroless bath. Neither surface type showed nickel plating (PEM with no Catalyst). Negatively charged SPS surfaces catalyzed with the negative palladium catalyst showed a very small nickel growth rate. After 25 minutes, the nickel was only 4.6 nm thick. These

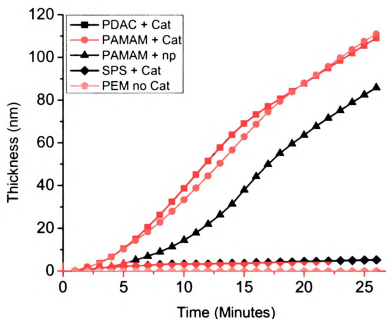


Figure 14: QCM data for homogeneous surfaces that represent the different regions on the patterned surfaces.

data suggest the interpenetration of PEM allows for a small amount of catalyst to adsorb on to the outer “SPS” surface.

Conclusion

The methods used to introduce the catalyst to the PEM surfaces before electroless deposition significantly affected the nickel pattern selectivity and resulting morphology. Directly stamping the catalyst yielded the highest selectivity. Encapsulating the catalyst inside PAMAM dendrimers slowed the plating rate and caused an agglomerated morphology. DA created excellent metal patterns but did not have a high selectivity. The decreased selectivity was caused by the interpenetration of the subsurface PEM layers into the outer polyelectrolyte layer. The effect of the subsurface layers was also demonstrated when the substrate effect on electroless nickel deposition was removed by increasing the PEM film thickness. The nickel patterning was affected by the substrate until more than five polyelectrolyte bilayers were deposited on the surface. Our approach of combining PEM, μ CP and ELD is versatile, inexpensive and allows for a wide variety of different substrates to be utilized. In addition, further modification of the surface is possible to add additional functionality or create bimetallic patterns.

Chapter 4: Direct Transfer of Patterned Polymer/Graphite Conductive Nanocomposite Films to Polyelectrolyte Multilayer Platforms

Introduction

LbL assembly of PEM has become a ubiquitous process for creating functional ultra thin films. Introduced by Decher, the simple deposition of two oppositely charged polyions can be performed on many types of surfaces giving them new functionality based on the type of polyelectrolytes utilized.¹ Incorporating new functional materials like nanoparticles, proteins or therapeutic chemicals can alter film properties and has lead to changes in mechanical,^{18, 28} surface wetting,^{4, 20} antireflective²⁴ and luminescent⁷⁸ properties and resulted in applications as biosensors^{79, 80} or drug delivery.^{81, 82} Exfoliated graphite has been incorporated into PEM and other polymer composite films for its unique mechanical, thermal and electrical properties which are comparable to carbon nanotubes.⁸³⁻⁸⁹ Multilayer graphite, large stacks of sp^2 hybridized graphene sheets bound together by weak van der Waals interactions, is an ideal starting material because it is inexpensive and available in large quantities. To take advantage of these properties, oxidized graphite has been incorporated into PEM.⁸⁶⁻⁸⁹ Oxidized graphite is created by the acid treatment of graphite which exfoliates the multilayered graphene sheets into platelets of only a few graphene layers thick, creates a negative charge so they are stable in aqueous solutions and renders the graphite nonconductive. LbL assembly with a positively charged polyelectrolyte allows for the formation of PEM. To make conductive films the oxidized graphite must be reduced back to graphite, which is not cost-effective

and can change the film morphology. To our knowledge no one has performed LbL assembly using exfoliated graphite which was not oxidized. Mass production of these films for optical or electronic devices requires a patterned film on the surface. Patterning a single layer of graphite does not have a large enough surface coverage to surpass the percolation threshold, which means a multilayer film is required for conductivity. Recently the direct transfer of multilayer films has been shown as a facile route to fabricate patterned films that would be difficult to form using other assembly and patterning methods.⁵⁵⁻⁵⁸

We present a simple method of creating patterned conductive multilayered polymer/graphene nanocomposite films using the LbL assembly of exfoliated graphite nanoplatelets (xGnPTM) and the direct transfer of these films to a substrate. Multilayered graphite was exfoliated followed by milling to create size controlled xGnP.⁸⁵ The xGnP were then coated with a negatively charged polymer to form a stable aqueous solution. The solution was then used for electrostatic LbL assembly, with a positively charged polyelectrolyte as the counter ion, onto the surface of an uncharged hydrophobic elastomeric stamp. Once the film was formed it was placed in direct contact with a substrate of the opposite charge to directly transfer the multilayer film. If enough layers of xGnP were adsorbed to the stamp, the LbL film became conductive. Before LbL assembly the elastomeric stamp is coated with a layer of polyelectrolyte using relatively weak hydrophobic interactions between the stamp and film. When the stamp is removed from the substrate the strong electrostatic interactions



between the oppositely charged film and substrate hold the multilayer film on the substrate.

Experimental Details

Materials: 6-carboxyfluorescein (6-CF) and nitrocellulose membranes (0.22 μm pore diameter) were purchased from Sigma-Aldrich (Milwaukee, WI) and used as received. Poly(allylamine hydrochloride) (PAH, Mw 60,000) was obtained from Polysciences, Inc. (Warrington, PA). Graphite Intercalate Compounds (GIC) were purchased from UCAR Inc. PDAC, SPS, PDMS and DI water were obtained as described in Chapter 2.

xGnP Preparation: xGnP are created using a process developed in the Composite Materials and Structures Center at MSU.⁹⁰ GIC which are acid intercalated graphite about 300 μm in size were expanded using microwave radiation. The microwaves cause the intercalated acids to evaporate quickly and expand the multilayered graphite. The expanded graphite is then ultrasonicated using a tip sonicator.⁹¹ This creates xGnP of ~ 15 μm in diameter and 5-10 nm in thickness. The size of the xGnP is then reduced to a ~ 1 μm diameter using ball milling.^{84, 85, 92} xGnP used in the following experiments were 5-10 nm in thickness with a 1 μm diameter. 0.1 g of xGnP was added to a 100 mL aqueous solution containing 0.01 M SPS and 0.1 M NaCl. The solution was then tip sonicated using a Virtis Virsonic 100 for 30 min, agitated with stirring for 24 h and filtered using nitrocellulose membranes. The SPS coated xGnP were then redispersed in 100 mL of DI water and tip sonicated for 20 min. After sonication, any undispersed nanoplatelets on the surface of the solution were removed by

skimming the surface with wax paper. This xGnP/SPS solution was then used for LbL assembly.

Film Preparation on PDMS: PDMS stamps were fabricated by pouring as described in Chapter 2. The stamps were then placed in a 0.05 M solution of PAH at a pH of 10 for 20 min. The samples were then alternately dipped by hand into the xGnP-SPS solution (described above) and a solution containing 0.01 M PDAC and 0.1 M NaCl. The polymer dipping time was 20 min which was followed by two 5 min washing steps in water before the next polymer layer was adsorbed. Typically 4 or 6 bilayers were used for patterning. These samples have a positively charged outer PDAC surface.

Substrate Film Preparation: (PDAC/SPS)₁₀ PEM films with a SPS outer surface were fabricated as described in Chapter 3.

Transfer Printing: The coated stamps were removed from the washing solution and gently dried with nitrogen. The PDAC on the stamp was misted with DI water from a spray bottle and placed in conformal contact with the outer SPS surface on the PEM coated substrate. After one hour of contact time the stamp was removed and the xGnP containing film transferred to the surface due to the strong electrostatic forces.

Characterization: Optical and fluorescence microscope images were obtained as described in Chapter 3. 6-CF was dissolved in 0.1 M NaOH and used to selectively bind to positively charged regions on the surface. SEM images were obtained using a JOEL 6400V microscope equipped with a LaB₆ filament and operated at 8k eV. The conductivity of the samples was measured using

Impedance Spectroscopy. Two copper tape electrodes were attached to the surface of the film and the resistance (R) was measured. The resistances were normalized by the dimensions of the films and reported as a surface resistance ($\rho_s=R \cdot L/D$) where L is the length between the electrodes and D is the width of the electrode.

Results and Discussion

Our process is illustrated in **Figure 15**. Multilayered graphite was expanded using acid intercalation, followed by exfoliation using ultrasonication^{84, 91, 93} and

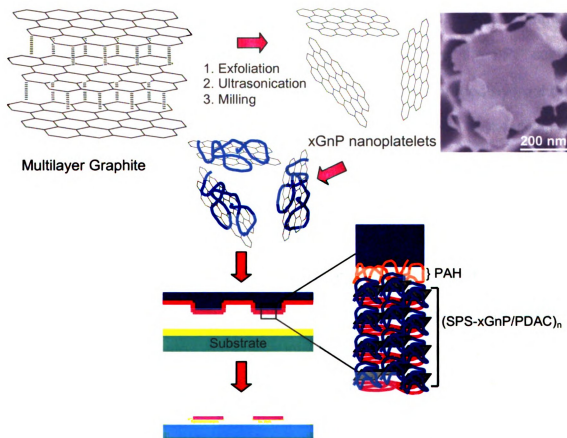


Figure 15: Illustration of the process to form xGnP, subsequent film formation on PDMS and transfer to a PEM coated substrate.

finally milled to create xGnP nanoplatelets (few layer graphene particles with a thickness of 5-10 nm and a 1 μm diameter). Since graphite is naturally hydrophobic, the xGnP need to be further modified to be used in LbL assembly from aqueous solutions. To solve this problem, ultrasonication was used to disperse the xGnP in a solution containing a negatively charged polymer (sulfonated polystyrene, SPS). The SPS coats the xGnP through interactions between the sp^2 hybridized graphitic surface and the aromatic rings of the polymer.⁹⁴ This coating facilitates the formation of a stable aqueous solution by preventing agglomeration of the xGnP through like charge repulsion. This charge also enables the xGnP-SPS to be used for electrostatic LbL assembly. Zeta potential measurements confirm the negative charge of the SPS coated xGnP. Before LbL assembly, topographically patterned uncharged hydrophobic poly(dimethylsiloxane) (PDMS) stamps were coated with poly(allylamine hydrochloride) (PAH) using hydrophobic interactions at a high pH. The PDMS substrates were then placed into a solution containing SPS coated xGnP, where the xGnP electrostatically deposits onto the PAH coated surface. After washing the sample is then placed into a solution containing positively charged poly(diallyldimethylammonium chloride) (PDAC) where a second layer deposits on the surface. Repeated immersion into the xGnP-SPS and PDAC solutions creates multilayer films denoted as $\text{PAH}/(\text{xGnP-SPS/PDAC})_n$ where n is the number of bilayers deposited on the PAH coated surface. The build up of multilayered films was confirmed by the gradually increasing darkness of the deposited film. PDAC was typically the final layer adsorbed. After the film was

fabricated it was removed from solution, gently blown dry and placed in contact with a negatively charged PEM coated substrate. Contact times were typically one hour. However it was found to be critical for the film to be completely dry before the stamp was removed from the substrate. The direct transfer of the multilayers proved to be more reproducible than directly microcontact printing the xGnP-SPS solution. It was possible to obtain patterns of xGnP using microcontact printing; however the process was less reproducible and observation from an optical microscope showed the patterns would not be conductive.

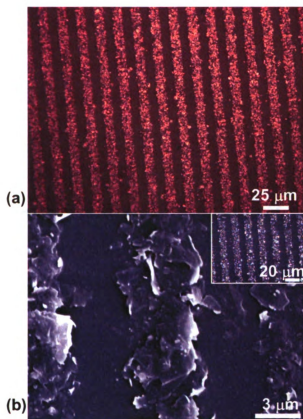


Figure 16: (a) Optical microscope and (b) SEM images of PAH/(xGnP-SPS/PDAC)₄ films transferred to a PEM coated substrate.

Figure 16 shows optical and scanning electron microscope (SEM) images of the transferred patterns of the PAH/(xGnP-SPS/PDAC)₄ composite films. Films containing 4 and 6 bilayers could be patterned on areas as large as the stamp (1.5cm x 3cm) using this technique. In the SEM image, **Figure 16b**, the xGnP are observed in multilayer stacks created by the LbL process. Additionally, the xGnP appear to be packed densely enough on the surface to conduct electrical current. AFM analysis shows that the transferred 4 and 6 bilayer films have a thickness of 85 nm and 120 nm respectively.

To ensure complete film transfer from the stamp, we used 6-carboxyfluorescein (6-CF), a negatively charged green fluorescent dye, to adsorb on surface of the xGnP containing films. **Figure 17a** shows the surface of a PDMS stamp that was placed in a 6-CF solution before patterning. The bright green dye was seen on both the peaks and valleys of the patterned stamp. A second stamp was also placed in the dye after patterning. Since the PAH/(xGnP-SPS/PDAC)₄ film was transferred to the surface, the dye can only be seen in inset regions of the stamp surface in **Figure 17b**. The film on the large homogeneous area to the right transfers due to sagging of the stamp. The optical microscope image, **Figure 17c**, also confirms that there were no xGnP remaining on the raised regions of the stamp.

The electrical properties of the films were determined by measuring the surface resistance. **Figure 18** displays the results of our measurements. Uncoated PDMS substrates and two bilayers on PDMS were found to be nonconductive. (Samples on PDMS were measured without the final layer of PDAC.) However,

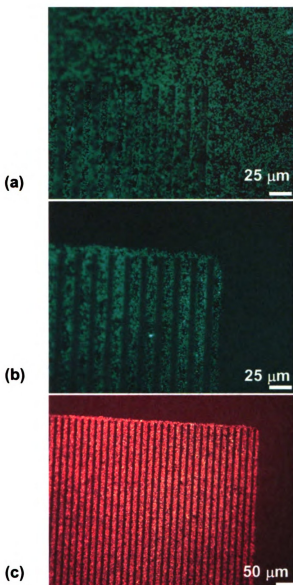


Figure 17: Fluorescence microscope images of PDMS stamps coated with PAH/(xGnP-SPS/PDAC)₄ films and dyed with 6CF (a) before and (b) after stamping. (c) An optical microscope image of a stamp after the film is transferred.

when four bilayers are used, the percolation threshold is surpassed and the samples are found to be conductive. Six bilayer films on PDMS show the lowest surface resistance of $5.8 \times 10^4 \Omega/\text{sqr}$. This resistance is comparable to previous reports using oxidized graphite to make the film.⁸⁶ However, we use a smaller

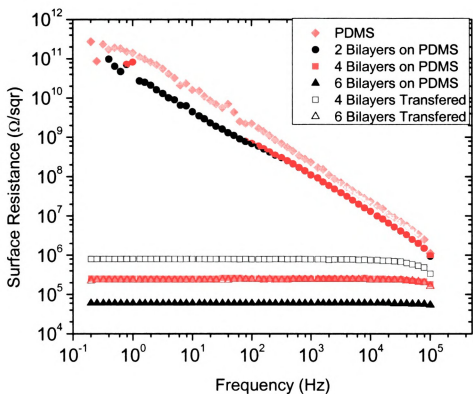


Figure 18: Surface resistance vs. Frequency for various films on PDMS and films transferred to PEM surfaces.

number of layers, six instead of ten, to achieve nearly the same resistance. Four and six bilayer films were transferred from PDMS to PEM coated glass slides. The surface resistance of these films increased slightly. The increase in resistance is caused by the presence of the dense 4-5 nm PAH layer which covers the xGnP-SPS layer.^{10, 55} We have attempted to lower the resistance of the transferred films by removing the layer of PAH. Soaking the samples in a high pH solution to cause charge screening and removal of the PAH was unsuccessful. Additionally plasma treatment did not remove the PAH layer. Heating the samples to 275°C for 3 hours and 10 minutes to burn out the

polymers also did not lower the measured resistance of the transferred six bilayer films.

Conclusion

In conclusion we report a novel method to create and pattern conductive polymer/graphene multilayered nanocomposite films using the combination of LbL assembly and direct transfer. Conductive polymer/graphene films were created on PDMS stamps with out the use of an oxidation step. By first adsorbing a weakly bound PAH layer onto a PDMS stamp the entire multilayer film can be completely transferred to a PEM coated substrate. This allows for these patterned films to be transferred to nearly any surface. The transferred films exhibit conductivity. However further increasing the conductivity and measurement of the films anisotropic conductivity associated with the patterns remain as future work.

Chapter 5: Control and Prevention of Polymer Film Buckling for Anti-wrinkling Applications

Introduction

Buckling or wrinkling is a natural phenomenon which occurs in numerous forms on different length scales.⁹⁵ Common forms of buckling include the wrinkling of human skin, the surface of many dried fruits, and even the formation of mountain ranges. Buckling occurs when a film resting on an elastic foundation is compressed. Recently there have been many reports on controlling the buckling morphology of thin metal or silica films on elastic or viscoelastic foundations.⁹⁶⁻¹⁰¹ For many thin film applications buckling can be an undesired result. However none of these buckling studies attempted to prevent buckling from occurring. The prevention of wrinkles caused by aging is of enormous interest to the cosmetics industry.¹⁰² For the first time we studied the control and prevention of buckling in PEM films induced by thermal processing or mechanical compression. We demonstrate the ability to control the PEM morphology and have successfully prevented the film from buckling by incorporating nanoparticles into the film.

PEM coatings can be used on any surface to significantly alter the surface properties.^{1, 30} As discussed in Chapter 1, the ultra thin polyelectrolyte layers add chemical functionality and change the surface morphology (i.e., thickness, surface roughness and porosity). The film morphology can be controlled by polyelectrolyte selection, the deposition conditions during assembly (e.g., salt concentration^{3, 8-10} and solution pH^{3, 12}) and the film formation procedure.³ Rubner and coworkers have shown that for a weak polyelectrolyte system, acid treatment after film formation creates a porous film morphology.^{14, 15} For

practical applications a permanent film morphology and functionality is desired and can be created by crosslinking the PEM thin film coatings.¹⁰³ The formation of covalent bonds between the multilayers has been used to create, cell adhesion layers,¹⁰⁴ anti-corrosion films¹⁰⁵ and organic thin-film transistors¹⁰⁶ as well as protein resistant surfaces on PDMS.²⁶ However, a buckled PEM film morphology has not previously been permanently created, spatially controlled, or prevented, by creating compressive forces from the substrate.

Internal compressive stresses caused thermally or mechanically in thin films or their substrates cause the formation of buckles. Buckling has been observed for metal films on top of an elastomeric substrate or film.^{97, 100, 101} A compressive stress is generated by either heating or cooling, and results in the isotropic buckling of the metal film. The generation of a silica layer (up to 500 nm in thickness) on a PDMS substrate and a compressive force, created thermally or mechanically, has also been used to create a buckled surface morphology.^{96, 98, 99} The buckling of multilayered polymer films on stiff substrates due to a change in humidity or temperature has also been demonstrated.¹⁰⁷ A patterned composite PEM film has been shown to buckle in two stages due to adjacent regions having two different Young's moduli.¹⁰⁸ This was done by applying enough compressive force to buckle stiffer regions while the more elastic regions remained unbuckled. When a greater amount of stress is applied the entire film buckled. The buckling of polymer films has also been used to measure their physical properties.^{109, 110} This was done at room temperature by applying a reversible external compressive force to the substrate in one dimension that

causes the polymer film to buckle in a sinusoidal wave pattern. By measuring the buckling wavelength (λ) and film thickness (d), the Young's modulus (E) of the film can be calculated by using Equation 1.

$$\lambda = 2\pi d \left(\frac{E_f (1 - \nu_s^2)}{3E_s (1 - \nu_f^2)} \right)^{\frac{1}{3}} \quad (1)$$

where ν is the Poisson's ratio and the subscripts s and f refer to the substrate and film, respectively. Further studies have shown that this technique can also be used to find the effective and individual modulus of multiple films composed of more than one material (e.g., polystyrene and PEM) on top of a PDMS substrate.^{111, 112} The effective modulus is found by treating the multiple layers as one composite film. Of the few studies on polymer films, none of them have shown spatial control over the buckling morphology or attempted to prevent the buckling from occurring.

In our work we present methods to create, spatially control, and prevent permanently buckled PEM films on flat PDMS substrates. The wrinkling is caused by the release of compressive stress created by heating the substrate and allowing it to cool. This thermal cycling can be an irreversible process creating internal stress which induces a permanently buckled morphology.¹¹³ Control over the film buckling morphology is demonstrated by varying the film thickness and the surface topography of the substrate. Additionally the effects of plasma treatment and the critical temperature for permanent buckling were studied. Using the knowledge we obtained, the prevention of permanent buckling was demonstrated for the first time, by adding nanoparticles to the films.

Experimental Details

Materials: Silica nanoparticles (50 ± 10 nm in a 5.65% aqueous solution) were obtained from Polysciences, Inc. (Warrington, PA). Solution pH was adjusted using 1.0 M HCl or NaOH. PDMS, PAH, PAA, PDAC, SPS and DI water are all obtained as described in previous chapters.

Sample Preparation: Flat PDMS substrates were created by curing the degassed prepolymer and initiator (10:1) mixture against a flat silicon wafer in an oven overnight at 60°C. The PDMS substrates were plasma cleaned (Harrick Scientific Corporation, Broadway Ossining, NY) with oxygen at ~0.150 Torr to make their surface hydrophilic. Glass microscope slides were cleaned as described in Chapter 1. Silicon wafers were cleaned in piranha solution for one hour and then plasma treated with oxygen for 4 minutes. A Carl Zeiss slide stainer was used to deposit PEM on the plasma cleaned substrates. The substrates were alternately dipped into a polycationic solution followed by washing in water. The substrate was then dipped into a polyanionic solution followed by washing to create one bilayer. The dipping cycle was repeated to form multilayer films. Two polyion pairs were used, PAH/PAA and PDAC/SPS. The PAH and PAA solutions were 0.01 M (concentration is based on the molecular weight of the polymer repeat unit) and the solution pH was adjusted to 7.5 and 3.5, respectively. The PDAC solution was 0.02 M and the SPS solution was 0.01M. Both solutions contained 0.1 M NaCl and the final solution pH was not adjusted.

Thermal Processing: The films were thermally processed by placing PEM coated substrates in a preheated oven for two hours. Unless otherwise stated

the oven temperature was set to 180°C. The samples were removed from the oven and allowed to cool to room temperature on the laboratory bench top.

Silica Nanoparticle Deposition: PEM were deposited as described above. When a layer of silica nanoparticles was deposited, the samples were removed from the slide stainer and manually drop-coated. Silica nanoparticles were diluted to a 0.5 % wt solution in water. The particles were drop-coated onto the surface for 30 minutes. Then samples were washed with water and gently blown dry with nitrogen. The slides were then placed back in the slide stainer for adsorption of additional polyelectrolyte layers.

Characterization: Optical microscope and AFM images were obtained as described in Chapter 2. Root mean square (RMS) roughness was measured by taking the average of at least 7 measurements of a 2.5 μm square box. The buckling wavelength was measured by taking the average of at least 7 peak to peak distances of parallel segments. Amplitude was calculated by measuring the height difference between the highest and lowest point of at least 7 different line scans and dividing by 2. PEM film thicknesses on silicon and PDMS substrates were measured using spectroscopic ellipsometry on an M-44 ellipsometer (J.A. Woolam Co., Inc.). It has been shown that there is enough contrast in refractive index between PDMS and PEM to accurately measure the film thickness.¹¹⁰

Results and Discussion

Silica Film Buckling: The RMS roughness of the PDMS substrates was comparable to the roughness of a silicon wafer (<0.5 nm). The repeating unit of PDMS, $-\text{OSi}(\text{CH}_3)_2-$, creates a hydrophobic surface with an advancing water contact angle of 108° .¹¹⁴ Treating the surface with oxygen plasma destroys the methyl groups, $\text{Si}-\text{CH}_3$, and forms a silica layer, SiO_x or $\text{Si}-\text{OH}$, which is hydrophilic.^{63, 114} When plasma treated PDMS is exposed to air low molecular

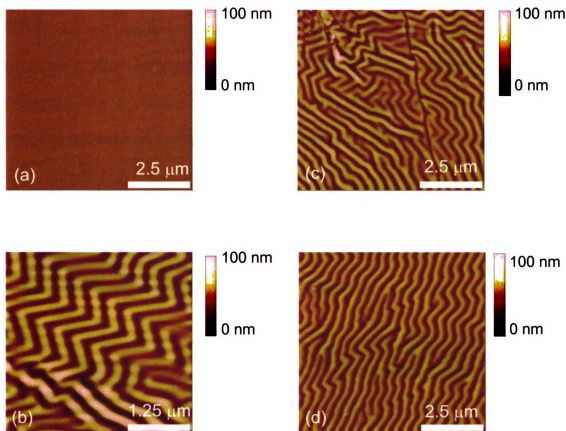


Figure 19: AFM images of flat PDMS substrates after (a) plasma treatment only, (b) plasma treatment and thermal processing the same day, (c) plasma treatment and overnight storage in air followed by thermal processing and (d) plasma treatment and storage in DI water overnight followed by thermal processing.

weight hydrophobic units ($-\text{CH}_3$) migrate to the surface increasing the contact angle. Placing the sample in water after oxidation can retard the regeneration of the hydrophobic surface.^{63, 114} Previous studies have shown that oxygen plasma treatment and a shift in temperature (either intentional⁹⁶ or unintentional⁹⁸) can cause the thin silica layer to buckle. It was not completely clear whether oxygen plasma treatment alone or the combination of plasma treatment and a temperature change would cause the PDMS film to buckle. To investigate whether the wrinkled morphology was caused while the silica layer was being generated, we tested bare PDMS substrates. The thermal processing of pure PDMS did not result in buckling. After oxygen plasma treating a flat PDMS substrate at room temperature, AFM was used to image the surface. As shown in **Figure 19a**, a plasma treated PDMS surface showed no change in surface morphology and had the same RMS roughness as an untreated PDMS substrate.

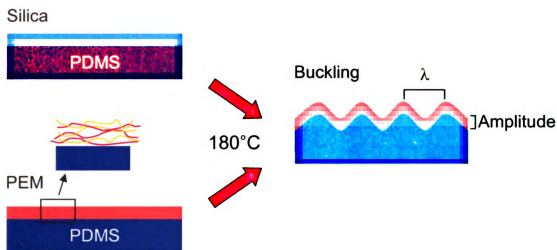


Figure 20: Cross-sectional illustration of a silica film generated by oxygen plasma treatment (top) and a PEM film (bottom), before and after thermal processing.

Then we thermally processed the plasma treated PDMS substrates, as illustrated in **Figure 20**. These samples include plasma treatment followed by thermal processing in the same day (**Figure 19b**), plasma treatment followed by storage overnight in either air (**Figure 19c**) or DI water (**Figure 19d**) and thermal processing the next day. All samples with plasma treatment buckled only after thermal processing. This means both plasma treatment and thermal processing are responsible for the buckling phenomena. The buckling data for oxygen plasma treated PDMS substrates are summarized in **Table 2**. The sample that was thermally processed the same day as plasma treatment exhibited a smaller wavelength than the samples that were processed the next day. This behavior is caused by a higher Young's modulus due to a shorter time between plasma treatment and thermal processing. Less time between plasma treatment and thermal processing means the surface will have a more silica like layer without the lower modulus hydrophobic material that migrates to the surface over time. The amplitude and wavelength of the buckles in our system are much smaller than a previously demonstrated morphology created with a thermal processing step.⁹⁶ Due to the similar refractive indices of the silica layer and PDMS, 1.46 and 1.44, respectively it was not possible to measure the thickness of the silica layer on top of PDMS using an ellipsometer. Instead, we used Equation 1 to determine the average thickness for the silica layer. An average silica layer thickness of 3.11 ± 0.3 nm was determined using $\nu_f = 0.33$, $\nu_s = 0.5$, $E_f = 70$ GPa and $E_s = 1.8$ MPa. This value is lower than expected based on previously reported values.^{96, 98} We believe that the temperature dependence of the

modulus was the cause for our unsatisfactory result.¹¹⁵ Previous buckling studies with significant temperature shifts were also unsuccessful in calculating the correct modulus when the modulus has previously been determined.^{96, 97}

Table 2: Summary of buckling data for plasma treated PDMS substrates with no PEM films

<i>additional surface treatment</i>	<i>RMS roughness (nm)</i>	<i>wavelength (nm)</i>	<i>amplitude (nm)</i>
none (plasma only)	0.22 ± 0.03		
TP ^a same day	18.9 ± 12.3	386.0 ± 40.2	37.4 ± 6.2
air storage, TP next day	15.0 ± 2.2	453.9 ± 24.5	34.5 ± 7.9
DI storage, TP next day	10.7 ± 0.7	460.8 ± 36.9	18.3 ± 2.5

^a TP = Thermal Processing

Crosslinkable PEM Film Buckling: Crosslinkable PEM films, (PAH/PAA)_{5.5}, were deposited onto flat plasma treated PDMS substrates. The RMS roughness for our PEM film on PDMS measured by AFM was 1.83 ± 0.98 nm. After film formation the samples were thermally processed (see **Figure 20**). This type of thermal processing is commonly used to crosslink PEM films composed of PAH/PAA.¹⁰³ When the samples were removed from the oven, the films were optically clear for a couple of minutes. This means there was no necking or crazing that occurred because of the thermal expansion of the PDMS substrate. However, after cooling the samples became translucent indicating a change in the film morphology. Optical microscope and AFM images, shown in **Figure 21**, confirm the morphology change of these films. The RMS roughness of the PEM

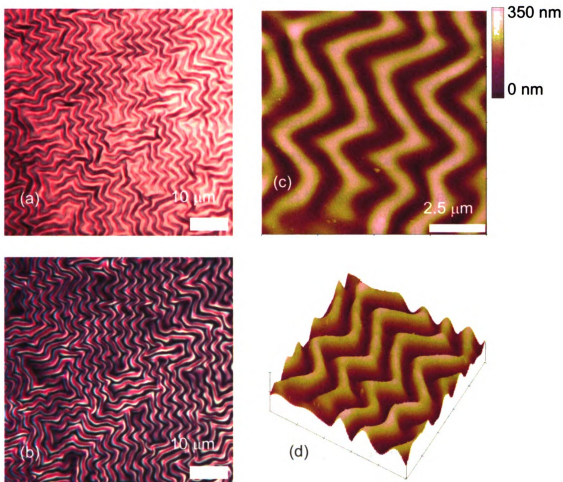


Figure 21: Optical microscope and AFM images of a buckled (PAH/PAA)_{5.5} film on a PDMS substrate after thermal processing. The smooth buckling morphology is caused by a mismatch in thermal expansion between the film and the substrate. (a) bright-field and (b) dark-field optical microscope images. (c) and (d) are 2D and 3D tapping mode AFM images, respectively.

films increased considerably to 77.43 ± 14.10 nm. For the same films on glass slides there was no morphology change after thermal processing, the PEM film remained optically clear and the RMS roughness did not change. This suggests that the new wavelike morphology was the result of having a PEM film on top of PDMS and not due the crosslinking of the film. An isotropic bi-axial compressive stress caused by a mismatch in the thermal expansion coefficients between the

thin PEM film and the elastomeric PDMS substrate. As the temperature increases from room temperature to 180°C, the surface area of the PDMS substrate increases ~20 % (using a $3.0 \times 10^{-4} \text{ } ^\circ\text{C}^{-1}$ coefficient of thermal expansion for PDMS).⁹⁶ While heated the PEM film may expand with the substrate and rearrange on the PDMS surface. This expansion and rearrangement may cause a reduction in the film thickness along with creating a small number of micron-sized cracks in the PEM film where the PDMS surface was exposed. While expanded, no necking or crazing of PEM film was observed. At the elevated temperature of 180°C, the PAH/PAA film begins to crosslink. As more time passes the film completes crosslinking and becomes more rigid and polyimide-like. When the sample was removed from the oven the surface area of the PDMS substrate begins to decrease back to its original size at room temperature. Due to the strong adhesion between the rigid PEM film and the

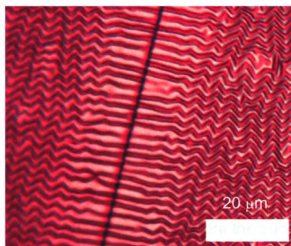


Figure 22: Optical microscope image a micro-crack in a (PAH/PAA)_{5.5} film. Compressive stress is released at the film crack and affected the film buckling morphology for ~15 mm.

PDMS substrate, the film was isotropically compressed and begins to buckle and form the randomly ordered wavelike morphology, as shown in **Figure 21**. No delamination of the PEM films was observed after heating or cooling. However there was some cracking of the films surface as show in **Figure 22** of the supporting materials. This kind of cracking is commonly observed for buckling of thin films.^{65, 96, 99} We theorize that the observed buckling in **Figure 21** is the buckling of a two plate composite film¹¹¹ where the silica film and PEM film jointly buckle at the same wavelength. Utilizing Equation 1, we calculated an effective modulus of 225 ± 56 MPa for the silica-PEM composite film where $\nu_f = 0.33$, and d is the thickness of the silica-PEM film. This value is significantly lower than the value previously reported for PAH/PAA assembled under the same pH conditions.¹¹¹ This happened because Equation 1 does not account for the temperature dependence of the Young's modulus.¹¹⁵ The calculated modulus may also be low because the film thickness may decrease when the PDMS surface expands during the thermal processing.

Non-Crosslinkable PEM Buckling: To further explore the wrinkling phenomenon, we employed a second PEM film. Non-crosslinkable PDAC/SPS films with different thicknesses were formed on PDMS and thermally processed. **Figure 23** shows that the periodic buckling of PDAC/SPS on PDMS does occur for films over a range of thicknesses. Furthermore the buckling was not a result of thermal crosslinking but instead was caused by the difference in coefficients of thermal expansion. The number of bilayers in the PDAC/SPS films was varied to observe the effect of the film thickness on the wrinkled film morphology that was

observed after thermal processing. **Figure 23** shows AFM images of 10, 20 and 40 bilayer PDAC/SPS films. In agreement with Equation 1, the wavelength of the buckles in these films changes linearly with the film thickness. The RMS roughness and buckling amplitude also increase linearly with the film thickness. This means that by depositing the appropriate number of polyelectrolyte bilayers onto a PDMS surface, the RMS roughness, amplitude and wavelength of the buckled film can be controlled. The $(\text{PDAC/SPS})_{20}$ and $(\text{PAH/PAA})_{5.5}$ films have a similar thickness, 98.6 nm and 75.4 nm respectively, before thermal processing.

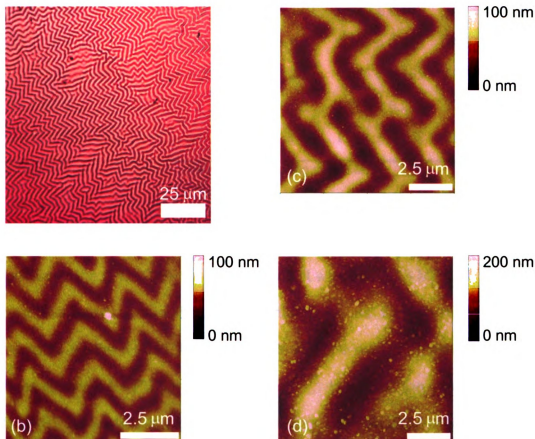


Figure 23: Optical microscope and AFM images of a buckled PDAC/SPS films on PDMS substrates after thermal processing. The smooth wavelike morphology is observed again but now for a film that is not known to crosslink. (a) Optical microscope image of a $(\text{PDAC/SPS})_{20}$ film. (b) – (d) tapping mode AFM images of 10, 20 and 40 bilayer PDAC/SPS films respectively.

However the amplitude of the buckled films was drastically different after the same amount of compressive stress from thermal processing was applied to the samples (see **Table 3**). The thicker film, (PDAC/SPS)₂₀, has a smaller amplitude than the (PAH/PAA)_{5.5} film. This is characteristic of a stiffer (i.e., higher Young's modulus)

Table 3: Summary of buckling data for PEM films on PDMS substrates

<i>surface</i>	<i>thickness (nm)</i>	<i>RMS roughness (nm)</i>	<i>wavelength (μm)</i>	<i>amplitude (nm)</i>
(PAH7.5/PAA3.5) _{5.5}	75.4 ± 6.1	77.4 ± 14.1	1.549 ± 0.103	147.4 ± 16.9
(PDAC/SPS) ₁₀	51.0 ± 7.8	11.7 ± 0.8	0.861 ± 0.840	24.8 ± 3.2
(PDAC/SPS) ₂₀	98.6 ± 2.0	16.7 ± 2.6	1.976 ± 0.165	40.3 ± 3.5
(PDAC/SPS) ₄₀	190.2 ± 0.7	24.7 ± 6.3	4.008 ± 0.211	77.8 ± 8.7
PAH(SPS/PDAC) _{19.5} ^a	82.1 ± 5.3	127.3 ± 5.0	1.911 ± 0.148	234.6 ± 16.1

^a Plasma treatment was not used before depositing the PEM.

film. Additionally when Equation 1 was used to calculate the effective Young's modulus of the (PDAC/SPS)₂₀ film, the result was 208 ± 13 MPa. This value was about the same, within the experimental error, as the effective modulus we calculated for the (PAH/PAA)_{5.5} film but is still one order of magnitude lower than values reported for PEM systems.^{65, 110, 111, 116} However, the observation that the PDAC/SPS film has a higher modulus than the PAH/PAA film agrees with a report where a PAH/PAA film with more elongated polymer chains, like

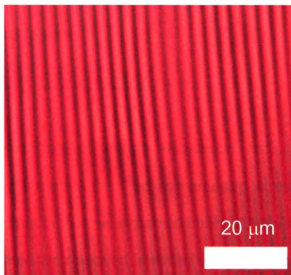


Figure 24: Optical microscope image of the manually compressed $(\text{PDAC/SPS})_{20}$ film. The average wavelength was found to be $3.26 \mu\text{m}$.

PDAC/SPS, exhibited a higher modulus than PAH/PAA film with more loopy polymer chains.¹¹⁶ To further understand the behavior of our system, we manually compressed a $(\text{PDAC/SPS})_{20}$ film and obtained the one dimensional buckles described previously.¹⁰⁹⁻¹¹² We determined the buckling wavelength to be $3.26 \mu\text{m}$ (see **Figure 24**) which was larger than the wavelength produced by thermal processing. Using Equation 1, we determined the modulus of a $(\text{PDAC/SPS})_{20}$ film to be $929 \pm 57 \text{ MPa}$. This value is slightly less than previously reported values for a $(\text{PAH/SPS})_{20}$ film.⁶⁵ We also observed that after compression the PEM film on the pinched sample did not immediately become flat. Buckles on the surface were still observed a half an hour after compression. However after two hours the sample appeared completely flat under the optical microscope.

Critical Buckling Temperature: The compressive stress, σ , in the PEM film can be calculated as follows;¹¹³

$$\sigma = \frac{E_f(\alpha_s - \alpha_f)}{(1 - \nu_f)} \Delta T \quad (2)$$

where α is the coefficient of thermal expansion and ΔT is the difference in maximum and final temperature. The compressive stress was a result of the difference in coefficient of thermal expansion between the film and the substrate.

When the substrates are removed from the oven and the temperature begins to decrease, the PDMS begins to compress the stiff upper film. However the film does not immediately bend until the stress reaches a critical value where the film will finally begin to buckle. This critical stress can be calculated using Equation 3.^{117, 118}

$$\sigma_c = \sqrt[3]{\frac{9}{64} \frac{E_s^2 E_f}{(1 - \nu_s^2)^2 (1 - \nu_f^2)}} \quad (3)$$

The critical compressive stress, σ_c , is dependent on the physical properties (i.e., Young's modulus and Poisson's ratio) of the film and substrate. Once the film buckles the modulus can be calculated using Equation 1. Our system is somewhat more complicated than the one described here since ours is a two plate composite film.

We experimentally estimated the critical temperature for permanent film buckling of a (PDAC/SPS)₂₀ film by changing the maximum temperature of the thermal processing. We tested samples at maximum thermal processing temperatures ranging between 50 and 180°C. When samples are heated to a

maximum temperature of 115°C, no permanent buckling occurred. However at 120°C or more buckling occurred. We determined the critical buckling temperature for permanent film buckling to be ~118°C. This translates to a critical stress for permanent film buckling of ~3 % linear strain for a (PDAC/SPS)₂₀ film. We theorize when a PEM film on PDMS was heated to a maximum temperature above 118°C and then cooled the process was reversible with no permanent effects on the film morphology (i.e., no permanent buckling). However once the maximum temperature of thermal processing ≥120°C, the process was irreversible which causes the PEM film to permanently buckle.

Effects of Silica Layer Absence: We further studied the effect of the silica layer created by plasma treatment on the buckling morphology. PDAC/SPS can not be assembled on a hydrophobic (non-plasma treated) surface. However by starting with one layer of PAH, at a pH of 7.5, SPS/PDAC can be assembled on PDMS, where PAH interacts with PDMS by hydrophobic interactions and SPS/PDAC can be built on the PAH by electrostatic interactions.⁵⁶ We created a twenty bilayer film with a first layer of PAH and 19.5 bilayers of SPS/PDAC, denoted as PAH (SPS/PDAC)_{19.5} in **Table 3**. This film has a thickness of 81.3 ± 5.3 nm before thermal processing. After thermal processing, the PAH (SPS/PDAC)_{19.5} film buckled as shown in **Figure 25**. The amplitude of this film was nearly six times larger than the (PDAC/SPS)₂₀ film. The increase in amplitude was caused by the absence of the silica layer created during plasma treatment that removes a significant amount of the compressive stress applied to the film from the PDMS substrate. The buckling wavelength does not change

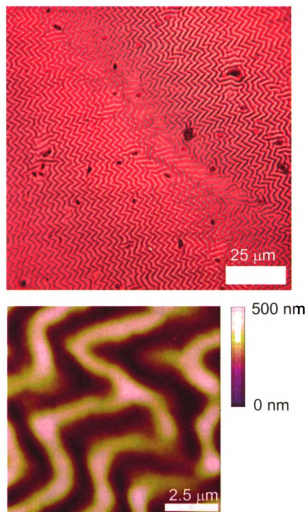


Figure 25: Optical microscope and AFM images of a PAH(SPS/PDAC)_{19.5} film on PDMS with no plasma treatment before multilayer assembly. The amplitude of the waves is high because there is no SiO₂ layer to help absorb the compressive strain.

much between these two films. This suggests the PAH(SPS/PDAC)_{19.5} film under goes a different amount of thinning during expansion of the PDMS than a (PDAC/SPS)₂₀ film due to the weaker hydrophobic interactions between the PDMS substrate and the PEM films. This difference in expanded film thickness may cause the films to buckle at the same wavelength even though their effective moduli are different.

Surface Topography Effects: The buckled PEM morphology was spatially controlled or prevented by varying the physical topography of the PDMS surface, as shown in **Figure 26**. We deposited (PAH/PAA)_{5.5} bilayers onto patterned PDMS substrates. The patterned PDMS surfaces contained 2.6 μm high circular columns spaced 18 μm apart (center to center distance) with varying diameters from 1.25 to 9 μm . The PEM coated PDMS was then thermally processed for 2 hours. As shown in **Figure 26**, the PEM film made a transition from disordered isotropic film buckling (flat PDMS) into a highly ordered buckled morphology (patterned PDMS). This order was caused by the release of the compressive

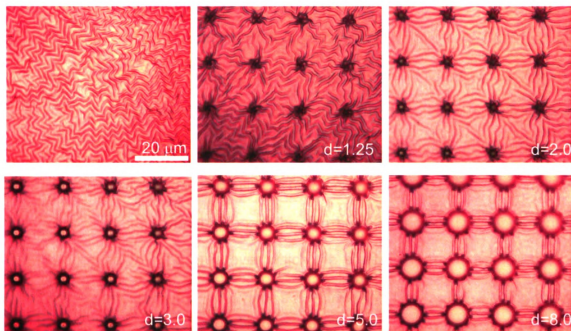


Figure 26: Optical microscope images of a (PAH/PAA)_{5.5} film on a topographically patterned PDMS substrate after thermal processing. The column diameter determines whether the buckled film is ordered ($d > \lambda$) or randomly oriented ($d < \lambda$). The scale bar is valid to all images.

stress in the PEM film at the column.^{96, 97} The stress was completely released in a direction perpendicular to the columns while the compressive stress in a direction tangent to the column is only partially decreased. This causes the film at the columns to only be compressed in one direction. When compared to the flat PDMS surface, the presence of the 1.25 μm diameter columns increased the wavelength of the PEM film from 1.55 μm to 2.2 μm due to a reduction in the compressive stress. However, the column diameter was still smaller than the buckling wavelength of the film on a flat surface; hence the buckling was still randomly oriented. Once the column diameter was greater than the flat surface buckling wavelength ($d \geq 2 \mu\text{m}$), the wrinkles begin and end at the columns. At a diameter of 4 μm and above (i.e., larger than the buckling wavelength) the polymer wrinkles only connected at contiguous columns. As the diameter increased further, the number of wrinkles between contiguous columns decreased and the size of the relatively unbuckled region between the columns increased. The presence of surface topography also decreased the number of micron-sized cracks in the PEM film. The cracks in homogeneous films reduced the stress and altered orientation of the film buckling similar to changes in the PDMS topography. The area over which the stress was released and the film buckling was affected was $\sim 15 \mu\text{m}$ for a (PAH/PAA)_{5.5} film (as seen in **Figure 22**).

Prevention of Buckling: Since the buckling of the film due to thermal processing is usually an undesirable result for many thin film applications, we set out to prevent the wrinkling from occurring for the first time. We observed that physical obstacles (i.e., surface topography) in a film affected the initiation and

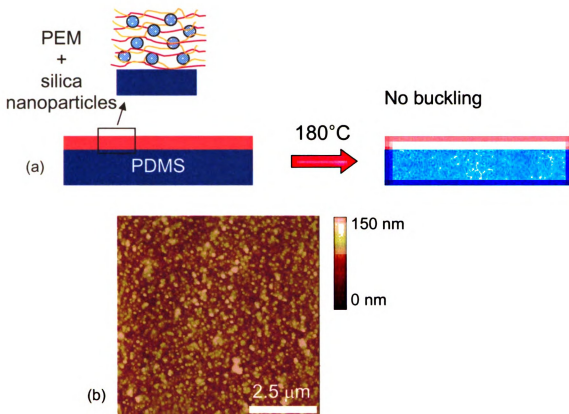


Figure 27: (a) Schematic illustration of the composite nanoparticle/polyelectrolyte film, $(\text{PDAC}/\text{SiO}_2(\text{PDAC}/\text{SPS})_4)_4$, film before and after thermal processing. (b) AFM image of the film after thermal processing. The addition of nanoparticles alleviates the compressive stress and prevents buckling.

orientation of the film buckling that occurs around them. For this reason we hypothesized that the incorporation of nanoparticles may act like a change in the surface topography and perturb the generation of film buckling induced by thermal processing. Our use of PEM films made this a very simple process since the incorporation of functional nanomaterials into a PEM film is widespread.³⁰ We selectively replaced layers of SPS in a $(\text{PDAC}/\text{SPS})_{20}$ film with monolayers of 50 nm negatively charged silica (SiO_2) nanoparticles. As illustrated in Scheme 1,

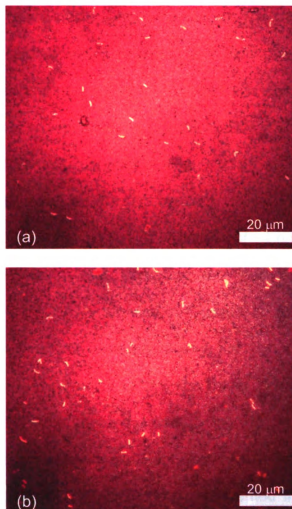


Figure 28: Optical microscope images of the composite nanoparticle/polyelectrolyte film, $(\text{PDAC}/\text{SiO}_2(\text{PDAC}/\text{SPS})_4)_4$ (a) before and (b) after thermal processing. The addition of nanoparticles alleviates the compressive stress and prevents buckling.

uniform layers on PDMS composed of silica (up to 500 nm), PEM, or stacked layers of silica and PEM buckle after thermal processing. The challenge was to integrate silica and PEM to obtain the physical morphology of a mixed film that does not buckle. To prevent the buckling, first, a single layer of nanoparticles was added at three different positions in the film. The SPS layer in bilayer 1, 10 or 20 was replaced with nanoparticles and thermally processed. The addition of a single layer of nanoparticles, however, did not prevent the film from buckling,

possibly due to low nanoparticle surface coverage. The coverage of each layer deposition of silica nanoparticles was not that high due to the electrostatic repulsion of the individual nanoparticles. Another film was created where SPS was replaced by SiO₂ nanoparticles in bilayers 1, 6, 11, and 15 abbreviated as [PDAC/SiO₂(PDAC/SPS)₄]₄ (illustrated in **Figure 27a**). An increased number of silica nanoparticle layers within the film resulted in an increase in nanoparticle surface coverage. Due to a small bilayer thickness of ~4 nm, nanoparticles from different deposition layers were deposited in different nanoscopic planes throughout the entire film. As evidenced in **Figure 27b** most nanoparticles are evenly distributed in films, but some aggregates are also observed. **Figure 28** shows optical microscope images of the film taken before and after thermal processing and confirms that there was no buckling. Because of the nanometer size of silica particles, the films are still optically transparent. The incorporation of 4 layers of nanoparticles into the PEM film prevented the film from buckling after thermal processing. According to Equations 2 and 3 adding silica nanoparticles into the film will increase the effective modulus and decrease the critical stress required for buckling. The effective modulus of the mixed films should be between the values of silica and PEM films. Since both homogeneous silica and PEM films buckled, it was very surprising to find that the mixed film did not buckle. We believe the presence of the nanoparticles in the film breakup and alleviate the compressive stress around the nanoparticles in the film so that buckling does not occur. In addition, the buckle-free films were mechanically compressed at room temperature. In a limited region, a small number of buckles

were observed propagating from the micron sized cracks. This means that most of the buckling was alleviated or prevented due to the presence of the nanoparticles.

Conclusion

We have shown the creation of buckled PEM films on flat PDMS substrates after thermal processing or mechanical compression. The buckling was caused by the release of compressive stress from the PDMS substrate. The thermally induced stress was created by the significant difference in coefficients of thermal expansion between the PEM film and PDMS substrate. The effect of the silica layer created after plasma treatment has been studied. Control over the film morphology (i.e., buckling) was demonstrated by controlling the film thickness and physical topography of the PDMS substrate. For the first time film buckling was prevented by the addition of silica nanoparticles. We believe this was because the compressive stress, which causes buckling, was decreased (or dissipated) and isotropically dispersed by the nanoparticles in the film. Future studies will include the use of various nanoparticle film compositions (i.e., number of nanoparticle layers and nanoparticle sizes) to prevent the film buckling with less material and/or smaller film thicknesses.

References

1. Decher, G. Fuzzy nanoassemblies: Toward layered polymeric multicomposites. *Science* **277**, 1232-1237 (1997).
2. Quinn, J. F., Johnston, A. P. R., Such, G. K., Zelikin, A. N. & Caruso, F. Next generation, sequentially assembled ultrathin films: Beyond electrostatics. *Chemical Society Reviews* **36**, 707-718 (2007).
3. Clark, S. L., Montague, M. F. & Hammond, P. T. Ionic effects of sodium chloride on the templated deposition of polyelectrolytes using layer-by-layer ionic assembly. *Macromolecules* **30**, 7237-7244 (1997).
4. Krogman, K. C., Zacharia, N. S., Schroeder, S. & Hammond, P. T. Automated process for improved uniformity and versatility of layer-by-layer deposition. *Langmuir* **23**, 3137-3141 (2007).
5. Izquierdo, A., Ono, S. S., Voegel, J. C., Schaaff, P. & Decher, G. Dipping versus spraying: Exploring the deposition conditions for speeding up layer-by-layer assembly. *Langmuir* **21**, 7558-7567 (2005).
6. Chiarelli, P. A., Johal, M. S. et al. Controlled fabrication of polyelectrolyte multilayer thin films using spin-assembly. *Advanced Materials* **13**, 1167-1171 (2001).
7. Cho, J., Char, K., Hong, J. D. & Lee, K. B. Fabrication of highly ordered multilayer films using a spin self-assembly method. *Advanced Materials* **13**, 1076-1078 (2001).
8. Harris, J. J. & Bruening, M. L. Electrochemical and in situ ellipsometric investigation of the permeability and stability of layered polyelectrolyte films. *Langmuir* **16**, 2006-2013 (2000).
9. Ladam, G., Schaad, P. et al. In situ determination of the structural properties of initially deposited polyelectrolyte multilayers. *Langmuir* **16**, 1249-1255 (2000).
10. Park, J. & Hammond, P. T. Polyelectrolyte multilayer formation on neutral hydrophobic surfaces. *Macromolecules* **38**, 10542-10550 (2005).
11. Yoo, D., Shiratori, S. S. & Rubner, M. F. Controlling bilayer composition and surface wettability of sequentially adsorbed multilayers of weak polyelectrolytes. *Macromolecules* **31**, 4309-4318 (1998).
12. Shiratori, S. S. & Rubner, M. F. Ph-dependent thickness behavior of sequentially adsorbed layers of weak polyelectrolytes. *Macromolecules* **33**, 4213-4219 (2000).

13. Mendelsohn, J. D., Yang, S. Y., Hiller, J., Hochbaum, A. I. & Rubner, M. F. Rational design of cytophilic and cytophobic polyelectrolyte multilayer thin films. *Biomacromolecules* **4**, 96-106 (2003).
14. Mendelsohn, J. D., Barrett, C. J. et al. Fabrication of microporous thin films from polyelectrolyte multilayers. *Langmuir* **16**, 5017-5023 (2000).
15. Hiller, J., Mendelsohn, J. D. & Rubner, M. F. Reversibly erasable nanoporous anti-reflection coatings from polyelectrolyte multilayers. *Nature Materials* **1**, 59-63 (2002).
16. Clark, S. L. & Hammond, P. T. The role of secondary interactions in selective electrostatic multilayer deposition. *Langmuir* **16**, 10206-10214 (2000).
17. Chen, J. Y., Luo, G. B. & Cao, W. X. The study of layer-by-layer ultrathin films by the dynamic contact angle method. *Journal of Colloid and Interface Science* **238**, 62-69 (2001).
18. Hendricks, T. R. & Lee, I. Wrinkle-free nanomechanical film: Control and prevention of polymer film buckling. *Nano Letters* **7**, 372-379 (2007).
19. Cebeci, F. C., Wu, Z. Z., Zhai, L., Cohen, R. E. & Rubner, M. F. Nanoporosity-driven superhydrophilicity: A means to create multifunctional antifogging coatings. *Langmuir* **22**, 2856-2862 (2006).
20. Zhai, L., Cebeci, F. C., Cohen, R. E. & Rubner, M. F. Stable superhydrophobic coatings from polyelectrolyte multilayers. *Nano Letters* **4**, 1349-1353 (2004).
21. Bravo, J., Zhai, L., Wu, Z. Z., Cohen, R. E. & Rubner, M. F. Transparent superhydrophobic films based on silica nanoparticles. *Langmuir* **23**, 7293-7298 (2007).
22. Ahn, J. S., Hendricks, T. R. & Lee, I. Control of specular and diffuse reflection of light using particle self-assembly at the polymer and metal interface. *Advanced Functional Materials* **17**, 3619-3625 (2007).
23. Ahn, J. S., Hammond, P. T., Rubner, M. F. & Lee, I. Self-assembled particle monolayers on polyelectrolyte multilayers: Particle size effects on formation, structure, and optical properties. *Colloids and Surfaces a-Physicochemical and Engineering Aspects* **259**, 45-53 (2005).
24. Wu, Z. Z., Walish, J. et al. Deformable antireflection coatings from polymer and nanoparticle multilayers. *Advanced Materials* **18**, 2699-2702 (2006).

25. Ladam, G., Schaaf, P., Cuisinier, F. J. G., Decher, G. & Voegel, J. C. Protein adsorption onto auto-assembled polyelectrolyte films. *Langmuir* **17**, 878-882 (2001).
26. Makamba, H., Hsieh, Y. Y., Sung, W. C. & Chen, S. H. Stable permanently hydrophilic protein-resistant thin-film coatings on poly(dimethylsiloxane) substrates by electrostatic self-assembly and chemical cross-linking. *Analytical Chemistry* **77**, 3971-3978 (2005).
27. Caruso, F., Niikura, K., Furlong, D. N. & Okahata, Y. Assembly of alternating polyelectrolyte and protein multilayer films for immunosensing .2. *Langmuir* **13**, 3427-3433 (1997).
28. Mamedov, A. A., Kotov, N. A. et al. Molecular design of strong single-wall carbon nanotube/polyelectrolyte multilayer composites. *Nature Materials* **1**, 190-194 (2002).
29. Tang, Z. Y., Kotov, N. A., Magonov, S. & Ozturk, B. Nanostructured artificial nacre. *Nature Materials* **2**, 413-U418 (2003).
30. Hammond, P. T. Form and function in multilayer assembly: New applications at the nanoscale. *Advanced Materials* **16**, 1271-1293 (2004).
31. Jiang, C. Y. & Tsukruk, V. V. Freestanding nanostructures via layer-by-layer assembly. *Advanced Materials* **18**, 829-840 (2006).
32. Baude, P. F., Ender, D. A. et al. Pentacene-based radio-frequency identification circuitry. *Applied Physics Letters* **82**, 3964-3966 (2003).
33. Forrest, S. R. The path to ubiquitous and low-cost organic electronic appliances on plastic. *Nature* **428**, 911-918 (2004).
34. Smits, J. H. A., Meskers, S. C. J., Janssen, R. A. J., Marsman, A. W. & de Leeuw, D. M. Electrically rewritable memory cells from poly(3-hexylthiophene) schottky diodes. *Advanced Materials* **17**, 1169-1173 (2005).
35. Carmichael, T. B., Vella, S. J. & Afzali, A. Selective electroless metal deposition using microcontact printing of phosphine-phosphonic acid inks. *Langmuir* **20**, 5593-5598 (2004).
36. Geissler, M., Kind, H., Schmidt-Winkel, P., Michel, B. & Delamarche, E. Direct patterning of nib on glass substrates using microcontact printing and electroless deposition. *Langmuir* **19**, 6283-6296 (2003).
37. Hidber, P. C., Helbig, W., Kim, E. & Whitesides, G. M. Microcontact printing of palladium colloids: Micron-scale patterning by electroless deposition of copper. *Langmuir* **12**, 1375-1380 (1996).

38. Kind, H., Geissler, M. et al. Patterned electroless deposition of copper by microcontact printing palladium(ii) complexes on titanium-covered surfaces. *Langmuir* **16**, 6367-6373 (2000).
39. Moran, C. E., Radloff, C. & Halas, N. J. Benchtop fabrication of submicrometer metal line and island arrays using passive microcontact printing and electroless plating. *Advanced Materials* **15**, 804-807 (2003).
40. Wu, X. C., Bittner, A. M. & Kern, K. Spatially selective electroless deposition of cobalt on oxide surfaces directed by microcontact printing of dendrimers. *Langmuir* **18**, 4984-4988 (2002).
41. Bittner, A. M., Wu, X. C. & Kern, K. Electroless metallization of dendrimer-coated micropatterns. *Advanced Functional Materials* **12**, 432-436 (2002).
42. Geissler, M. & Xia, Y. N. Patterning: Principles and some new developments. *Advanced Materials* **16**, 1249-1269 (2004).
43. Xia, Y. N. & Whitesides, G. M. Soft lithography. *Angewandte Chemie-International Edition* **37**, 551-575 (1998).
44. Lee, I. S., Hammond, P. T. & Rubner, M. F. Selective electroless nickel plating of particle arrays on polyelectrolyte multilayers. *Chemistry of Materials* **15**, 4583-4589 (2003).
45. Mallory, G. O. & Hajdu, J. B. (eds.) *Electroless plating: Fundamentals & applications* (American Electroplaters and Surface Finishers Society, Orlando, FL, 1990).
46. Knez, M., Sumser, M. et al. Spatially selective nucleation of metal clusters on the tobacco mosaic virus. *Advanced Functional Materials* **14**, 116-124 (2004).
47. Kumar, A., Biebuyck, H. A. & Whitesides, G. M. Patterning self-assembled monolayers - applications in materials science. *Langmuir* **10**, 1498-1511 (1994).
48. Xia, Y. N., Mrksich, M., Kim, E. & Whitesides, G. M. Microcontact printing of octadecylsiloxane on the surface of silicon dioxide and its application in microfabrication. *Journal of the American Chemical Society* **117**, 9576-9577 (1995).
49. Kidambi, S., Chan, C. & Lee, I. S. Selective depositions on polyelectrolyte multilayers: Self-assembled monolayers of m-dpeg acid as molecular template. *Journal of the American Chemical Society* **126**, 4697-4703 (2004).

50. Jiang, X. P., Zheng, H. P., Gourdin, S. & Hammond, P. T. Polymer-on-polymer stamping: Universal approaches to chemically patterned surfaces. *Langmuir* **18**, 2607-2615 (2002).
51. Zheng, H. P., Rubner, M. F. & Hammond, P. T. Particle assembly on patterned "Plus/minus" Polyelectrolyte surfaces via polymer-on-polymer stamping. *Langmuir* **18**, 4505-4510 (2002).
52. Lee, I., Ahn, J. S., Hendricks, T. R., Rubner, M. F. & Hammond, P. T. Patterned and controlled polyelectrolyte fractal growth and aggregations. *Langmuir* **20**, 2478-2483 (2004).
53. Kohli, N., Dvornic, P. R., Kaganove, S. N., Worden, R. M. & Lee, I. Nanostructured crosslinkable micropatterns by amphiphilic dendrimer stamping. *Macromolecular Rapid Communications* **25**, 935-941 (2004).
54. Hendricks, T. R., Dams, E. E., Wensing, S. T. & Lee, I. Effects of catalyst introduction methods using pamam dendrimers on selective electroless nickel deposition on polyelectrolyte multilayers. *Langmuir* **23**, 7404-7410 (2007).
55. Park, J., Fouche, L. D. & Hammond, P. T. Multicomponent patterning of layer-by-layer assembled polyelectrolyte/nanoparticle composite thin films with controlled alignment. *Advanced Materials* **17**, 2575-2579 (2005).
56. Park, J. & Hammond, P. T. Multilayer transfer printing for polyelectrolyte multilayer patterning: Direct transfer of layer-by-layer assembled micropatterned thin films. *Advanced Materials* **16**, 520-525 (2004).
57. Kohli, N., Worden, R. M. & Lee, I. Intact transfer of layered, bionanocomposite arrays by microcontact printing. *Chemical Communications*, 316-318 (2005).
58. Kohli, N., Worden, R. M. & Lee, I. Direct transfer of preformed patterned bio-nanocomposite films on polyelectrolyte multilayer templates. *Macromolecular Bioscience* **7**, 789-797 (2007).
59. Wang, T. C., Chen, B., Rubner, M. F. & Cohen, R. E. Selective electroless nickel plating on polyelectrolyte multilayer platforms. *Langmuir* **17**, 6610-6615 (2001).
60. Guo, T. F., Chang, S. C., Pyo, S. & Yang, Y. Vertically integrated electronic circuits via a combination of self-assembled polyelectrolytes, ink-jet printing, and electroless metal plating processes. *Langmuir* **18**, 8142-8147 (2002).
61. Clark, S. L. & Hammond, P. T. Engineering the microfabrication of layer-by-layer thin films. *Advanced Materials* **10**, 1515-1519 (1998).

62. Jagannathan, R. & Krishnan, M. Electroless plating of copper at a low ph level. *Ibm Journal of Research and Development* **37**, 117-123 (1993).
63. Kim, J. J., Kim, S. K., Lee, C. H. & Kim, Y. S. Investigation of various copper seed layers for copper electrodeposition applicable to ultralarge-scale integration interconnection. *Journal of Vacuum Science & Technology B* **21**, 33-38 (2003).
64. McNally, P. J., Kanatharana, J. et al. Geometric linewidth and the impact of thermal processing on the stress regimes induced by electroless copper metallization for si integrated circuit interconnect technology. *Journal of Applied Physics* **96**, 7596-7602 (2004).
65. Khang, D. Y., Jiang, H. Q., Huang, Y. & Rogers, J. A. A stretchable form of single-crystal silicon for high-performance electronics on rubber substrates. *Science* **311**, 208-212 (2006).
66. Zhang, D. H., Ryu, K. et al. Transparent, conductive, and flexible carbon nanotube films and their application in organic light-emitting diodes. *Nano Letters* **6**, 1880-1886 (2006).
67. Hendricks, T. R. & Lee, I. A versatile approach to selective and inexpensive copper patterns using polyelectrolyte multilayer coatings. *Thin Solid Films* **515**, 2347-2352 (2006).
68. Radloff, C., Vaia, R. A., Brunton, J., Bouwer, G. T. & Ward, V. K. Metal nanoshell assembly on a virus bioscaffold. *Nano Letters* **5**, 1187-1191 (2005).
69. Kohli, N., Hassler, B. L. et al. Tethered lipid bilayers on electrolessly deposited gold for bioelectronic applications. *Biomacromolecules* **7**, 3327-3335 (2006).
70. Tjong, V., Wu, L. & Moran, P. M. Three-dimensional metallized features on polymeric substrates by microcontact printing. *Langmuir* **22**, 2430-2432 (2006).
71. Arrington, D., Curry, M. & Street, S. C. Patterned thin films of polyamidoamine dendrimers formed using microcontact printing. *Langmuir* **18**, 7788-7791 (2002).
72. Li, H. W., Kang, D. J., Blamire, M. G. & Huck, W. T. S. High-resolution contact printing with dendrimers. *Nano Letters* **2**, 347-349 (2002).
73. Scott, R. W. J., Wilson, O. M. & Crooks, R. M. Synthesis, characterization, and applications of dendrimer-encapsulated nanoparticles. *Journal of Physical Chemistry B* **109**, 692-704 (2005).

74. Scott, R. W. J., Ye, H. C., Henriquez, R. R. & Crooks, R. M. Synthesis, characterization, and stability of dendrimer-encapsulated palladium nanoparticles. *Chemistry of Materials* **15**, 3873-3878 (2003).
75. Ye, H. C., Scott, R. W. J. & Crooks, R. M. Synthesis, characterization, and surface immobilization of platinum and palladium nanoparticles encapsulated within amine-terminated poly(amidoamine) dendrimers. *Langmuir* **20**, 2915-2920 (2004).
76. Dressick, W. J., Dulcey, C. S., Georger, J. H., Calabrese, G. S. & Calvert, J. M. Covalent binding of pd catalysts to ligating self-assembled monolayer films for selective electroless metal-deposition. *Journal of the Electrochemical Society* **141**, 210-220 (1994).
77. Kind, H., Bittner, A. M., Cavalleri, O., Kern, K. & Greber, T. Electroless deposition of metal nanoislands on aminothioliolate-functionalized au(111) electrodes. *Journal of Physical Chemistry B* **102**, 7582-7589 (1998).
78. Mamedov, A. A., Belov, A., Giersig, M., Mamedova, N. N. & Kotov, N. A. Nanorainbows: Graded semiconductor films from quantum dots. *Journal of the American Chemical Society* **123**, 7738-7739 (2001).
79. Okamoto, Y., Kitagawa, F. & Otsuka, K. Online concentration and affinity separation of biomolecules using multifunctional particles in capillary electrophoresis under magnetic field. *Analytical Chemistry* **79**, 3041-3047 (2007).
80. Kohli, N., Srivastava, D. et al. Nanostructured biosensor for measuring neuropathy target esterase activity. *Analytical Chemistry* **79**, 5196-5203 (2007).
81. Berg, M. C., Zhai, L., Cohen, R. E. & Rubner, M. F. Controlled drug release from porous polyelectrolyte multilayers. *Biomacromolecules* **7**, 357-364 (2006).
82. Zelikin, A. N., Li, Q. & Caruso, F. Degradable polyelectrolyte capsules filled with oligonucleotide sequences. *Angewandte Chemie-International Edition* **45**, 7743-7745 (2006).
83. Stankovich, S., Dikin, D. A. et al. Graphene-based composite materials. *Nature* **442**, 282-286 (2006).
84. Cho, D., Lee, S., Yang, G. M., Fukushima, H. & Drzal, L. T. Dynamic mechanical and thermal properties of phenylethynyl-terminated polyimide composites reinforced with expanded graphite nanoplatelets. *Macromolecular Materials and Engineering* **290**, 179-187 (2005).

85. Kalaitzidou, K., Fukushima, H. & Drzal, L. T. Multifunctional polypropylene composites produced by incorporation of exfoliated graphite nanoplatelets. *Carbon* **45**, 1446-1452 (2007).
86. Kotov, N. A., Dekany, I. & Fendler, J. H. Ultrathin graphite oxide-polyelectrolyte composites prepared by self-assembly: Transition between conductive and non-conductive states. *Advanced Materials* **8**, 637-641 (1996).
87. Kovtyukhova, N. I., Ollivier, P. J. et al. Layer-by-layer assembly of ultrathin composite films from micron-sized graphite oxide sheets and polycations. *Chemistry of Materials* **11**, 771-778 (1999).
88. Cassagneau, T., Guerin, F. & Fendler, J. H. Preparation and characterization of ultrathin films layer-by-layer self-assembled from graphite oxide nanoplatelets and polymers. *Langmuir* **16**, 7318-7324 (2000).
89. Szabo, T., Szeri, A. & Dekany, I. Composite graphitic nanolayers prepared by self-assembly between finely dispersed graphite oxide and a cationic polymer. *Carbon* **43**, 87-94 (2005).
90. Fukushima, H. in *Chemical Engineering & Materials Science* (Michigan State University, East Lansing, MI, 2003).
91. Chen, G. H., Weng, W. G. et al. Preparation and characterization of graphite nanosheets from ultrasonic powdering technique. *Carbon* **42**, 753-759 (2004).
92. Kalaitzidou, K., Fukushima, H. & Drzal, L. T. A new compounding method for exfoliated graphite-polypropylene nanocomposites with enhanced flexural properties and lower percolation threshold. *Composites Science and Technology* **67**, 2045-2051 (2007).
93. Du, X. S., Xiao, M. & Meng, Y. Z. Synthesis and characterization of polyaniline/graphite conducting nanocomposites. *Journal of Polymer Science Part B-Polymer Physics* **42**, 1972-1978 (2004).
94. Stankovich, S., Piner, R. D. et al. Stable aqueous dispersions of graphitic nanoplatelets via the reduction of exfoliated graphite oxide in the presence of poly(sodium 4-styrenesulfonate). *Journal of Materials Chemistry* **16**, 155-158 (2006).
95. Genzer, J. & Groenewold, J. Soft matter with hard skin: From skin wrinkles to templating and material characterization. *Soft Matter* **2**, 310-323 (2006).

96. Bowden, N., Huck, W. T. S., Paul, K. E. & Whitesides, G. M. The controlled formation of ordered, sinusoidal structures by plasma oxidation of an elastomeric polymer. *Applied Physics Letters* **75**, 2557-2559 (1999).
97. Bowden, N., Brittain, S., Evans, A. G., Hutchinson, J. W. & Whitesides, G. M. Spontaneous formation of ordered structures in thin films of metals supported on an elastomeric polymer. *Nature* **393**, 146-149 (1998).
98. Chua, D. B. H., Ng, H. T. & Li, S. F. Y. Spontaneous formation of complex and ordered structures on oxygen-plasma-treated elastomeric polydimethylsiloxane. *Applied Physics Letters* **76**, 721-723 (2000).
99. Efimenko, K., Rackaitis, M. et al. Nested self-similar wrinkling patterns in skins. *Nature Materials* **4**, 293-297 (2005).
100. Kim, J. & Lee, H. H. Wave formation by heating in thin metal film on an elastomer. *Journal of Polymer Science Part B-Polymer Physics* **39**, 1122-1128 (2001).
101. Yoo, P. J., Suh, K. Y., Park, S. Y. & Lee, H. H. Physical self-assembly of microstructures by anisotropic buckling. *Advanced Materials* **14**, 1383-1387 (2002).
102. Chiu, A. & Kimball, A. B. Topical vitamins, minerals and botanical ingredients as modulators of environmental and chronological skin damage. *British Journal of Dermatology* **149**, 681-691 (2003).
103. Harris, J. J., DeRose, P. M. & Bruening, M. L. Synthesis of passivating, nylon-like coatings through cross-linking of ultrathin polyelectrolyte films. *Journal of the American Chemical Society* **121**, 1978-1979 (1999).
104. Picart, C., Elkaim, R. et al. Primary cell adhesion on rgd-functionalized and covalently crosslinked thin polyelectrolyte multilayer films. *Advanced Functional Materials* **15**, 83-94 (2005).
105. Dai, J. H., Sullivan, D. M. & Bruening, M. L. Ultrathin, layered polyamide and polyimide coatings on aluminum. *Industrial & Engineering Chemistry Research* **39**, 3528-3535 (2000).
106. Stricker, J. T., Gudmundsdottir, A. D., Smith, A. P., Taylor, B. E. & Durstock, M. F. Fabrication of organic thin-film transistors using layer-by-layer assembly. *Journal of Physical Chemistry B* **111**, 6322-6326 (2007).
107. Basu, S. K., Bergstreser, A. M., Francis, L. F., Scriven, L. E. & McCormick, A. V. Wrinkling of a two-layer polymeric coating. *Journal of Applied Physics* **98**, 063507 (2005).

108. Jiang, C., Singamaneni, S., Merrick, E. & Tsukruk, V. V. Complex buckling instability patterns of nanomembranes with encapsulated gold nanoparticle arrays. *Nano Letters* **6**, 2254-2259 (2006).
109. Stafford, C. M., Harrison, C. et al. A buckling-based metrology for measuring the elastic moduli of polymeric thin films. *Nature Materials* **3**, 545-550 (2004).
110. Nolte, A. J., Rubner, M. F. & Cohen, R. E. Determining the young's modulus of polyelectrolyte multilayer films via stress-induced mechanical buckling instabilities. *Macromolecules* **38**, 5367-5370 (2005).
111. Nolte, A. J., Cohen, R. E. & Rubner, M. F. A two-plate buckling technique for thin film modulus measurements: Applications to polyelectrolyte multilayers. *Macromolecules* **39**, 4841-4847 (2006).
112. Stafford, C. M., Guo, S., Harrison, C. & Chiang, M. Y. M. Combinatorial and high-throughput measurements of the modulus of thin polymer films. *Review of Scientific Instruments* **76**, 062207 (2005).
113. Freund, L. B. & Suresh, S. Thin film materials: Stress, defect formation of surface evolution (Cambridge University Press, New York 2003).
114. Morra, M., Occhiello, E. et al. On the aging of oxygen plasma-treated polydimethylsiloxane surfaces. *Journal of Colloid and Interface Science* **137**, 11-24 (1990).
115. Fujita, H. & Ninomiya, K. Dependence of mechanical relaxation spectra of linear amorphous polymers on the distribution of molecular weights. *Journal of Polymer Science* **24**, 233-260 (1957).
116. Pavour, P. V., Bellare, A., Strom, A., Yang, D. H. & Cohen, R. E. Mechanical characterization of polyelectrolyte multilayers using quasi-static nanoindentation. *Macromolecules* **37**, 4865-4871 (2004).
117. Allen, H. G. Analysis and design of structural sandwich panels (Pergamon Press, New York, 1969).
118. Volynskii, A. L., Bazhenov, S., Lebedeva, O. V. & Bakeev, N. F. Mechanical buckling instability of thin coatings deposited on soft polymer substrates. *Journal of Materials Science* **35**, 547-554 (2000).

MICHIGAN STATE UNIVERSITY LIBRARIES



3 1293 02956 6266